Table 1. Combination index value analysis by CalcuSyn software (version 2) of combination efficiency in human lung cancer cells

Cells	Gemcitabine (nmol/L)	OBP-301 (MOI)	Combination index	Synergy
H460	10	10	1.261	—
		20	1.405	—
		50	1.688	—
	30	10	0.996	±
		20	1.106	–
		50	1.349	—
	50	10	1.037	±
		20	1.104	–
		50	0.998	±
	70	10	0.87	+
		20	1.037	±
		50	0.793	++
	100	10	0.793	++
		20	0.785	++
		50	0.531	+++
H358	1	10	0.952	±
		20	0.812	++
		50	0.772	++
	3	10	0.713	++
		20	0.674	+++
		50	0.641	+++
	5	10	0.792	++
		20	0.828	++
		50	0.613	+++
	7	10	0.88	+
		20	0.812	++
		50	0.596	+++
	10	10	1.178	–
		20	0.948	±
		50	0.693	+++
H322	50	25	1.028	±
		50	0.941	±
		75	0.874	++
		100	1.033	±
	100	25	0.953	±
		50	0.842	++
		75	0.848	++
		100	0.938	±
	200	25	0.944	±
		50	0.856	+
		75	0.82	++
		100	0.979	±
	300	25	0.912	±
		50	1.024	±
		75	0.887	+
		100	0.887	+
	400	25	1.005	±
		50	0.975	±
		75	1.093	±
		100	0.938	±
	500	25	0.977	±
		50	0.97	±
		75	0.946	±
		100	1.154	–

NOTE: Range of combination index symbol descriptions: 0.3 to 0.7, +++, synergism; 0.7 to 0.85, ++, moderate synergism; 0.85 to 0.90, +, slight synergism; 0.90 to 1.10, ±, additive; 1.10 to 1.20, –, slight antagonism; 1.20 to 1.45, —, moderate antagonism.

results suggest that combination treatment with OBP-301 plus gemcitabine was effective in all cell lines tested.

We also assessed the morphologic changes in cells treated with either the combination modality or single agents. Phase-contrast images at 96 hours after OBP-301 infection showed the growth of cells to subconfluence without morphologic changes in the presence of gemcitabine, whereas a rapid loss of viability due to massive cell death, as evidenced by ballooning and floating cells, was evident when gemcitabine was combined with OBP-301 infection (Supplementary Fig. S2).[5]

Effects of Gemcitabine on Replication of OBP-301 in Human Lung Cancer Cells *In vitro*

We used quantitative real-time PCR and Western blotting to assess the effects of gemcitabine on replication of OBP-301 in the three lung cancer cell lines. H460, H322, and H358 cells were infected with OBP-301 at an MOI of 10, 25, and 20, respectively, and were then treated with 70, 100, and 3 nmol/L of gemcitabine at 24 hours after infection. Cells were harvested at the indicated time points after OBP-301 infection, and extracted DNA was subjected to assay. As shown in Fig. 2A, the increase in intracellular viral copy number of OBP-301 by 4 to 5 orders of magnitude was consistent with or without gemcitabine in both treatment regimens. A plateau was reached at ~48 hours after infection. Western blot analysis also showed that E1A expression following OBP-301 infection was not hindered by gemcitabine in three lung cancer cell lines (Fig. 2B). These results suggest that gemcitabine does not interfere with OBP-301 replication.

Cell Cycle Analysis following OBP-301 Infection in Human Lung Cancer Cells

To further explore the "greater than additive response" observed when cells were infected with OBP-301 followed by gemcitabine treatment, we carried out cell cycle analysis of these cells after OBP-301 infection by flow cytometric analysis of propidium iodide–stained cells, a measure of DNA content. As shown in Fig. 3A, the cell cycle distribution apparently changed compared with mock-infected cells at 24 hours after OBP-301 infection in all cell lines tested, although there was no increase in the sub-G_0-G_1 population indicating apoptotic cell death. The number of cells in S phase increased from 43.85% to 56.41% in H460 cells, from 46.72% to 67.09% in H322 cells, and from 38.22% to 57.67% in H358 cells (Table 2). These results suggest that OBP-301 is able to accumulate infected cells in S phase, which may render cells more sensitive to gemcitabine.

Changes in Cell Cycle Regulator Protein Expression following OBP-301 Infection

To clarify the mechanisms of cell cycle regulation by OBP-301, we analyzed the expression of proteins that have a crucial role in the cell cycle. H460, H322, and H358 cells were infected with OBP-301 at an MOI of 40, 100, and 80, and Western blot analysis was then done 24 hours later. As shown in Fig. 3B, expression levels of E2F1, as well as phosphorylated Akt, greatly increased after OBP-301 infection compared with the mock-infected controls in all three cell lines. p53 protein expression was not detectable in H460

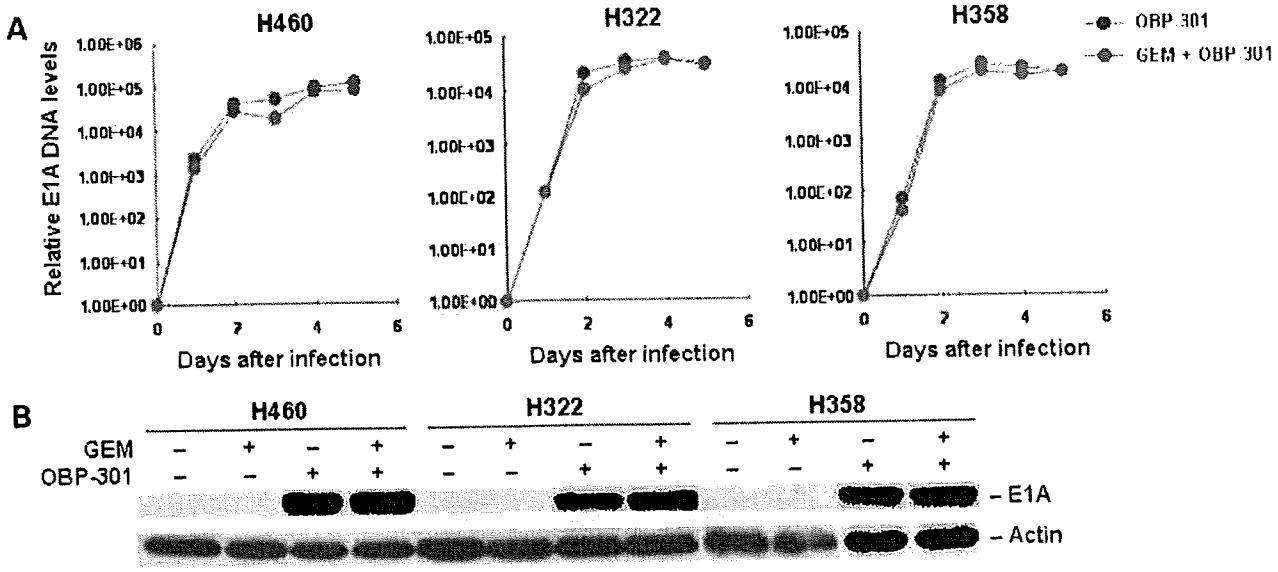

Figure 2. Assessment of viral DNA replication in human lung cancer cells. **A,** H460, H322, and H358 cells were infected with OBP-301 at an MOI of 10, 25, and 20, respectively, for 2 h as a baseline for virus DNA levels. Following the removal of virus inocula at 24 h after the infection, H460, H322, and H358 cells were further incubated with 70, 100, and 3 nmol/L of gemcitabine (*GEM*), respectively, for the indicated periods of time. Cells were then subjected to quantitative real-time PCR assay. Viral E1A copy number was defined as the fold increase for each sample relative to that at 2 h (2 h = 1). **B,** Western blot analysis of E1A expression in human lung cancer cells. Cells were treated with OBP-301, gemcitabine, or a combination of both, as described above, and then subjected to assay at 4 d after infection.

expressing the wild-type *p53* gene and p53-null H358 cells, whereas OBP-301 infection down-regulated mutant p53 expression in H322 cells.

Antitumor Effects of OBP-301 plus Gemcitabine in Human Lung Cancer Xenografts

Finally, we assessed the therapeutic efficacy of OBP-301 in combination with gemcitabine against H358 human lung cancer cells *in vivo*. H358 cells were implanted as xenografts into the hind flanks of *nu/nu* mice. Mice bearing palpable H358 tumors measuring 5 to 7 mm in diameter received simultaneous treatment of intratumoral injection of either 10^7 pfu OBP-301 or PBS plus i.p. administration of either 70 mg/kg gemcitabine or PBS every 3 days for three cycles starting at day 0. As shown in Fig. 4, administration of gemcitabine resulted in significant tumor growth suppression compared with mock-treated tumors for 34 days after initiation of treatment ($P < 0.05$); the combination of OBP-301 plus gemcitabine, however, produced a more profound and significant inhibition of tumor growth compared with mice treated with gemcitabine alone for at least 45 days ($P < 0.05$). The addition of OBP-301 clearly prolonged the antitumor effects of gemcitabine. Intratumoral injection of a replication-deficient adenovirus with or without systemic administration of gemcitabine had no apparent effect on the growth of H358 tumors (data not shown).

Discussion

Replication-competent oncolytic adenoviruses are promising as a novel anticancer therapy (9). In our laboratory, a tumor-specific replication-selective adenovirus, designated Telomelysin or OBP-301, is effective against human cancers (2–5). This virus was genetically designed to replicate under the control of hTERT promoter specifically in tumor cells, causing specific oncolysis. Despite the encouraging outcomes in animal experiments, combination chemotherapy and virotherapy are recommended in clinical treatment, as tumor progression is very rapid in most patients. In the current study, we explored the combination effects of OBP-301 and gemcitabine in human lung cancer cells *in vitro* and *in vivo*.

Adenovirus therapy combined with gemcitabine has been reported in the treatment of pancreatic cancer. Halloran et al. (9) reported that incubation of Panc-1 cells with either 5-fluorouracil or gemcitabine followed by adenovirus-mediated overexpression of $p16^{INK4A}$ resulted in a substantial reduction in cell viability under conditions where the drugs alone had minimal cytotoxicity. Although most studies reporting the combination effects of gemcitabine and adenoviral agents for pancreatic tumor used therapeutic genes critical for tumor growth inhibition, OBP-301 itself is an effective oncolytic virus and leads to infected cell destruction. Moreover, it has been reported that the type 5 adenoviral E1A sensitizes hepatocellular carcinoma cells to gemcitabine (10). These observations support the notion that oncolytic adenoviruses combined with gemcitabine are a rational modality for the treatment of human cancer.

The antitumor efficacy of OBP-301 was found to be enhanced when combined with gemcitabine in human lung cancer cells *in vitro* (Fig. 1; Table 1). Synergistic interaction was apparent in H460 and H358 cells; the combination

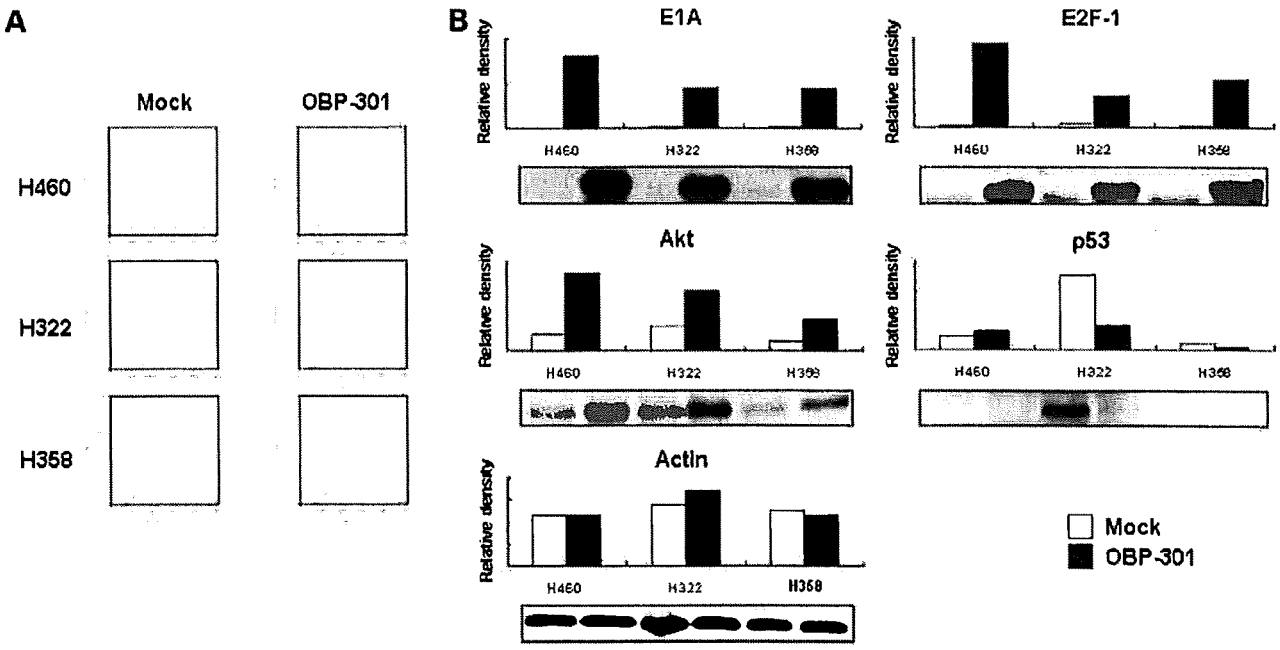

Figure 3. Cell cycle analysis and Western blotting of cell cycle regulator protein following OBP-301 infection in human lung cancer cells. **A,** H460, H322, and H358 cells were infected with OBP-301 at an MOI of 40, 100, and 80 MOI, respectively. DNA content was determined by propidium iodide staining and flow cytometric analysis at 24 h after OBP-301 infection. **B,** H460, H322, and H358 cells were either mock infected or infected with OBP-301 at an MOI of 40, 100, and 80 MOI, respectively. Following the removal of virus inocula, cells were collected at 24 h after infection and subjected to analysis. Equivalent amounts of protein obtained from whole-cell lysates were loaded into each lane, probed with primary antibodies, and then visualized using an enhanced chemiluminescence detection system. Equal loading of samples was confirmed by reprobing with antiactin antiserum. Protein expression was quantified by densitometric scanning using NIH Image software.

effect, however, was additive in H322 cells, suggesting that the effect of the combination is dependent on cell type. We also confirmed that this synergistic effect could be observed in human pancreatic cancer cells (Supplementary Fig. S3).[5] Gemcitabine is a deoxycytidine analogue and the incorporation of gemcitabine triphosphate into DNA causes chain termination, which is the major mechanism underlying the cytotoxicity of gemcitabine (11). Although there was concern over whether gemcitabine would interrupt the viral replication of OBP-301, quantitative real-time PCR analysis showed that intracellular replication of OBP-301 was not affected by gemcitabine (Fig. 2). The cytotoxic mechanisms of OBP-301 are distinct from those of gemcitabine, and therefore, combination effects could be observed provided that gemcitabine does not inhibit viral replication.

To clarify the mechanisms of the greater than additive response, cell cycle analysis was done following OBP-301 infection. Cells treated with OBP-301 tended to accumulate in the S phase at 24 hours after infection (Fig. 3A; Table 2). It has been reported that many DNA viruses can drive quiescent cells through G_1 into S phase by the expression of viral proteins (12–14). During the early phase of the adenovirus infection, the host cell is transformed into an efficient producer of the viral genome. The first gene that is transcribed in the viral genome is *E1A*, which can bind to numerous cellular proteins and acts as a multifunctional protein. Our data showed that OBP-301 infection increases the phosphorylation of Akt, as well as E2F1 expression, in all three human lung cancer cell lines (Fig. 3B). These effects are thought to be due to adenoviral E1A protein expression, as the dl312 adenovirus lacking the E1 genes did not phosphorylate Akt (data not shown).

Direct evidence of cell cycle promotion by Akt was seen when coexpression of Akt rescued cells from PTEN-induced cell cycle arrest (15). Retinoblastoma (Rb) protein restrains proliferation, in part, by modulating the activity of E2F

Table 2. Cell cycle analysis after OBP-301 infection in human lung cancer cells

Cell lines	Treatment	Cell cycle		
		G_1 (%)	S (%)	G_2 (%)
H460	Mock	43.54	43.85	8.61
	OBP-301	10.91	56.41	32.54
H322	Mock	40	46.72	10.85
	OBP-301	27.49	67.09	3.23
H358	Mock	45.89	38.22	14.29
	OBP-301	28.93	57.67	11.45

NOTE: H460, H322, and H358 cell lines were treated with OBP-301 at 40, 100, and 80 MOI, respectively. Cells were then subjected to cell cycle analysis at 24 h after treatment by the fluorescence-activated cell sorting method. The percentages of cells in the G_1, S, and G_2 phases are shown.

A

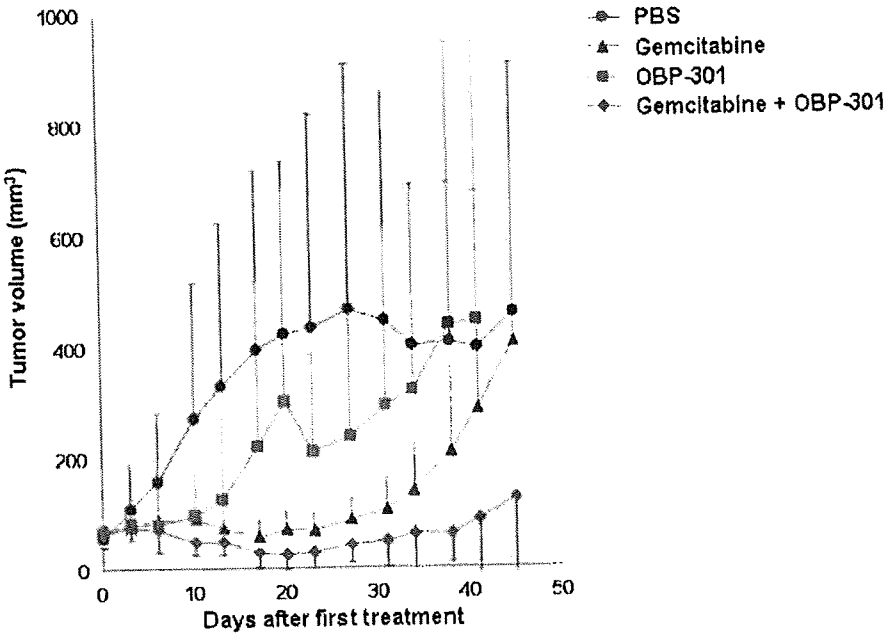

Figure 4. Antitumor effects of intratumorally injected OBP-301 and i.p. administered gemcitabine against established back H358 xenograft tumors in *nu/nu* mice. **A,** H358 tumor cells (5×10^6/each) were s.c. injected into the right flanks of mice. OBP-301 (1×10^8 pfu/body) and gemcitabine (70 mg/kg) were administered intratumorally and i.p., respectively, for three cycles every 3 d. PBS was used as the control. Eight mice were used for each group. Tumor growth is expressed as mean volume ± SE. **B,** statistical analysis was done using Student's *t* test for differences among indicated groups. Statistical significance (*red number*) was defined as $P < 0.05$.

B

	Day 23	Day 27	Day 31	Day 34	Day 38	Day 41	Day 45
PBS vs OBP-301	0.116	0.172	0.354	0.588	0.870	0.788	0.774
PBS vs Gemcitabine (GEM)	0.015	0.025	0.028	0.021	0.073	0.336	0.773
PBS vs GEM + OBP-301	0.009	0.014	0.014	0.005	0.004	0.008	0.051
OBP-301 vs GEM	0.034	0.068	0.101	0.155	0.198	0.377	0.594
OBP-301 vs OBP-301 + GEM	0.011	0.024	0.021	0.050	0.044	0.051	0.080
GEM vs OBP-301 + GEM	0.013	0.007	0.022	0.029	0.015	0.012	0.033

transcription factors. In quiescent cells, Rb associates with several E2Fs, resulting in the repression of proliferation-associated genes. As cells progress into the cell cycle, cyclin-dependent kinases phosphorylate Rb, freeing E2F and allowing it to directly transactivate genes required for S-phase entry (16). In fact, replication-deficient adenovirus-mediated *E2F1* gene transfer into human cancer cells resulted in accumulation of an S-phase cell population (Supplementary Fig. S4).[5] Thus, OBP-301 infection expressed E1A protein, which in turn up-regulated the expression of phosphorylated Akt and E2F1, leading to cell cycle promotion and S-phase entry presumably by the deactivation of Rb. Indeed, we confirmed that OBP-301 infection decreased Rb protein expression in H460 cells (data not shown). The accumulation of the tumor cells in S phase increases the cytotoxicity of gemcitabine, which kills cells in S phase.

In summary, our data show that telomerase-specific oncolytic adenovirus infection increases the sensitivity of human lung cancer cells to gemcitabine due to S-phase accumulation. The combination of OBP-301 and gemcitabine efficiently inhibits human cancer cell growth both *in vitro* and *in vivo*, an outcome that has important implications for tumor-specific oncolytic chemovirotherapies for human lung cancer.

Disclosure of Potential Conflicts of Interest

M. Ouchi, H. Onimatsu, and Y. Urata: employees of Oncolys BioPharma, Inc. T. Fujiwara: consultant for Oncolys BioPharma, Inc. No other potential conflicts of interest were disclosed.

Acknowledgments

We thank Daiju Ichimaru and Hitoshi Kawamura for their helpful discussions and Tomoko Sueishi for her excellent technical support.

References

1. Gkiozos I, Charpidou A, Syrigos K. Developments in the treatment of non-small cell lung cancer. Anticancer Res 2007;27:2823–7.

2. Kawashima T, Kagawa S, Kobayashi N, et al. Telomerase-specific replication-selective virotherapy for human cancer. Clin Cancer Res 2004;10:285–92.

3. Taki M, Kagawa S, Nishizaki M, et al. Enhanced oncolysis by a tropism-modified telomerase-specific replication-selective adenoviral agent OBP-405 ('Telomelysin-RGD'). Oncogene 2005;24:3130–40.

4. Hashimoto Y, Watanabe Y, Shirakiya Y, et al. Establishment of biological and pharmacokinetic assays of telomerase-specific replication-selective adenovirus. Cancer Sci 2008;99:385–90.

5. Endo Y, Sakai R, Ouchi M, et al. Virus-mediated oncolysis induces danger signal and stimulates cytotoxic T-lymphocyte activity via proteasome activator upregulation. Oncogene 2008;27:2375–81.

6. Khuri FR, Nemunaitis J, Ganly I, et al. A controlled trial of intratumoral ONYX-015, a selectively-replicating adenovirus, in combination with cisplatin and 5-fluorouracil in patients with recurrent head and neck cancer. Nat Med 2000;6:879–85.

7. Paz-Ares L, Douillard JY, Koralewski P, et al. Phase III study of gemcitabine and cisplatin with or without aprinocarsen, a protein kinase C-α antisense oligonucleotide, in patients with advanced-stage non-small-cell lung cancer. J Clin Oncol 2006;24:1428–34.

8. Heinemann V, Quietzsch D, Gieseler F, et al. Randomized phase III trial of gemcitabine plus cisplatin compared with gemcitabine alone in advanced pancreatic cancer. J Clin Oncol 2006;24:3946–52.

9. Halloran CM, Ghaneh P, Shore S, et al. 5-Fluorouracil or gemcitabine combined with adenoviral-mediated reintroduction of p16INK4A greatly enhanced cytotoxicity in Panc-1 pancreatic adenocarcinoma cells. J Gene Med 2004;6:514–25.

10. Lee WP, Tai DI, Tsai SL, et al. Adenovirus type 5 E1A sensitizes hepatocellular carcinoma cells to gemcitabine. Cancer Res 2003;63:6229–36.

11. Huang P, Chubb S, Hertel LW, Grindey GB, Plunkett W. Action of 2′,2-difluorodeoxycytidine on DNA synthesis. Cancer Res 1991;51:6110–7.

12. Wang HG, Draetta G, Moran E. E1A induces phosphorylation of the retinoblastoma protein independently of direct physical association between the E1A and retinoblastoma products. Mol Cell Biol 1991;11:4253–65.

13. Hollyoake M, Stühler A, Farrell P, Gordon J, Sinclair A. The normal cell cycle activation program is exploited during the infection of quiescent B lymphocytes by Epstein-Barr virus. Cancer Res 1995;55:4784–7.

14. Morozov A, Shiyanov P, Barr E, Leiden JM, Raychaudhuri P. Accumulation of human papillomavirus type 16 E7 protein bypasses G_1 arrest induced by serum deprivation and by the cell cycle inhibitor p21. J Virol 1997;71:3451–7.

15. Paramio JM, Navarro M, Segrelles C, Gomez-Casero E, Jorcano JL. PTEN tumor suppressor is linked to the cell-cycle control through the retinoblastoma protein. Oncogen 1999;18:7462–8.

16. Nahle Z, Polakoff J, Davuluri RV, et al. Direct coupling of the cell cycle and cell death machinery by E2F. Nat Cell Biol 2002;4:859–64.

Diagnostic potential and limitation of imaging cancer cells in cytological samples using telomerase-specific replicative adenovirus

YOSHIKO MAIDA[1], SATORU KYO[1], JUNKO SAKAGUCHI[1], YASUNARI MIZUMOTO[1], MANABU HASHIMOTO[1], NORIKO MORI[1], TOMOMI IKOMA[1], MITSUHIRO NAKAMURA[1], MASAHIRO TAKAKURA[1], YASUO URATA[2], TOSHIYOSHI FUJIWARA[3] and MASAKI INOUE[1]

[1]Department of Obstetrics and Gynecology, Kanazawa University, Graduate School of Medical Science, 13-1 Takaramachi, Kanazawa, Ishikawa 920-8641; [2]Oncolys BioPharma Inc., 3-16-33 Roppongi, Minato-ku, Tokyo 106-0032; [3]Center for Gene and Cell Therapy, Okayama University Hospital, 2-5-1 Shikata-cho, Okayama 700-8558, Japan

Received June 17, 2008; Accepted September 4, 2008

DOI: 10.3892/ijo_00000284

Abstract. Cytological cancer screening that targets genetic or epigenetic abnormalities may be a viable alternative to morphological screening. Detecting cancer cells by specific genetic markers helps their easy detection in cytological samples. We recently established the telomerase-specific replication-selective adenovirus OBP-401, in which the human telomerase reverse transcriptase (*hTERT*) gene promoter has been inserted upstream of the E1 genes, and in which the green fluorescent protein (*GFP*) gene is driven by the CMV promoter. This virus selectively replicates only in telomerase-positive cells, expressing GFP, and therefore may be a tool for cancer screening. In the present study, we first confirmed that cytological samples can easily be infected with OBP-401, allowing visualization of GFP-positive cells under fluorescent microscopy 24 h after infection. After 32 cytological samples from patients with cervical, endometrial or ovarian cancers were infected with OBP-401, GFP signals were detected in 31 (96%) of the samples. However, some normal endometrial scrapings exhibited GFP-signals, possibly due to endometrial glandular cells with constitutive telomerase activity. The ability of OBP-401 to enrich cancer cells was then tested. Cytological samples containing cervical or endometrial cancer cells were infected with OBP-401, and GFP-positive cells were sorted by flow cytometry; DNA was extracted from the GFP-positive cells. Direct DNA sequencing or methylation-specific PCR identified cancer-derived mutations or hypermethylations of tumor suppressor genes more efficiently than analyses using crude cytological samples. Thus, OBP-401-based sorting of GFP-positive cells successfully enriched cancer cells, allowing efficient detection of genetic or epigenetic abnormalities in cytological samples.

Correspondence to: Dr Satoru Kyo, Department of Obstetrics and Gynecology, Kanazawa University, School of Medical Science, 13-1 Takaramachi, Kanazawa, Ishikawa 920-8641, Japan
E-mail: satoruky@med.kanazawa-u.ac.jp

Key words: gynecologic cancers, cytological screening, molecular diagnosis, telomerase, adenovirus

Introduction

Molecular-based screening using cytological samples is an attractive alternative to morphological screening for the early detection of cancer. In molecular-based screening, the targets used to identify cancer cells are genetic abnormalities involved in carcinogenesis, such as gene mutations, deletion/insertion and chromosome loss/gain. Compared to RNA or protein, DNA is extremely stable irrespective of the viability of tumor cells, and therefore has an advantage as a screening target (1). In laboratory settings, PCR-based methods are commonly used to find genetic or epigenetic abnormalities. However, such methods are not very suitable for clinical cytological samples, because cytological samples are highly contaminated by normal cells, including not only stromal cells but inflammatory and blood cells, which interfere with detection of genetic abnormalities in cancer cells and thereby cause decreased sensitivity. For example, genetic analysis using exfoliated cells from the uterus has been unsuccessful, because of the high levels of mucous as well as blood and inflammatory cells present in samples from sexually active women. Thus, there is an urgent need for novel techniques that specifically enrich cancer cells from cytological samples.

One approach to cancer cell enrichment has been the use of immunomagnetic systems, in which antibodies against epithelial surface markers are linked to small paramagnetic microbeads, enabling target-cell selection using a powerful magnet (2-5). Many researchers have successfully used such systems for early detection of recurrent carcinomas, mainly using blood samples. However, such systems have not been useful for the screening of primary tumors, because of insufficient specificity in targeting of cancer cells.

Recently, we established a telomerase-specific replication-selective adenovirus (OBP-301, Telomelysin), in which the human telomerase reverse transcriptase (*hTERT*) promoter element has been inserted upstream of the *E1A* and *E1B* genes of the adenovirus type 5 genome (6) (Fig. 1A). Because the E1 protein is only produced in cancer cells via cancer-specific transactivation of the *hTERT* promoter (7-9), OBP-301 selectively replicates in a variety of human cancer cells. We then constructed the telomerase-specific replication-selective adenovirus OBP-401 (Telomelysin-GFP), in which the green fluorescent protein (GFP) gene has been inserted into the E3 region of the viral genome under the control of the cytomegalovirus (CMV) promoter (10). This chimera virus expresses GFP via viral replication only in telomerase-positive cancer cells, allowing selective visualization of cancer cells *in vitro* and *in vivo*. Kishimoto *et al* (11) reported successful *in vivo* imaging of lymph node metastasis in a mouse model of human rectal cancer, after injecting OBP-401 into the primary cancer sites. Thus, it appears that OBP-401 could be a useful tool for molecular imaging in cytological screening of cancer cells. In the present study, we used OBP-401 to detect and enrich cancer cells in cytological samples from gynecologic tissues.

Materials and methods

Cell culture and sample collection. Human cervical cancer C33A, HeLa and normal human fibroblast BJ cells were incubated in Dulbecco's modified Eagle's medium (DMEM) with 10% fetal bovine serum (FBS) in a 5% CO_2 atmosphere at 37°C.

Cytological samples were obtained from 61 patients who underwent cytological screening for detection of gynecologic malignancies at the Department of Obstetrics and Gynecology, Kanazawa University Hospital, between October 2005 and November 2006. Written informed consent was obtained from all patients. Of those 61 patients, 29 patients were normal controls who were undergoing annual cancer screening or whose chief complaint was abnormal genital bleeding. The cervical and endometrial scrapings of those normal controls were diagnosed as cytologically normal, and half of each control's scrapings used in the present analyses. The remaining 32 patients had histologically confirmed gynecologic cancers: 15 cervical cancers, 14 endometrial cancers, 2 vaginal stump cancers and 1 ovarian cancer. Cervical, endometrial or vaginal scrapings or ascite samples were obtained from those 32 patients, and were used in the present analyses. All scraping samples were brushed into DMEM with 10% FBS, and were incubated at 37°C in a 5% CO_2 atmosphere. Cellular viability was assessed by trypan blue staining using the ViCell cell counter system (Beckman Coulter, Fullerton, CA).

Infection with OBP-401 and observation of GFP-positive cells. OBP-401 was purified by ultracentrifugation in cesium chloride step gradients, and the titer was determined by plaque assay in 293 cells, as described previously (10). To optimize infectious conditions, C33A, HeLa and BJ cells were plated on dishes and infected with OBP-401 at multiplicities of infection (MOI) ranging from 0.01 to 10. After incubation for 24 h, GFP expression was visually assessed using an inverted fluorescence microscope.

To optimize infectious conditions of suspended cells, C33A and HeLa cells adjusted to $2x10^5$ cells were suspended in 50 μl of medium, and were incubated with 0.01-10 MOIs of OBP-401 for 1 h. Then, 50 μl of medium was added, and the cells were incubated for an additional 24 h. Next, 10 μl of the suspension was dropped on a glass slide, a cover glass was added, and GFP expression was visually assessed under fluorescence microscopy.

Pre-clinical sensitivity assay for screening of cancer cells. C33A cells were stained with CellTracker Blue CMAC (Invitrogen, Carlsbad, CA) according to the manufacturer's protocol. Blue-stained C33A cells were mixed with normal cervical scraping cells in cell suspensions at ratios ranging from 1:1 to 1:100000, and the total number of cells in each suspension was adjusted to $2x10^5$. Those cell suspensions were then incubated with OBP-401 at 10 MOI for 24 h, and then a 1/20 volume of each suspension was used for visual assessment of GFP expression. The blue-stained and green-fluorescent cells in non-diluted and 10-fold-diluted samples were counted in 10 randomly selected fields at a magnification of x100. For samples at higher dilutions, blue-stained and green-fluorescent cells were counted in all fields at a magnification of x100.

GFP-based sorting for genetic/epigenetic analyses. C33A cells were mixed with normal cervical scraping cells at a ratio of 1:9 or 1:1, and each mixture was divided into 2 tubes. The cells in one tube were incubated with OBP-401 at 10 MOI for 24 h. Then, GFP-positive cells in that tube were sorted by FACS using the EPICS ALTRA system (Beckman Coulter). In the other tube, which was used as a control, the cells were incubated without OBP-401 for 24 h. Genomic DNA was extracted from the cells in both tubes, and was subjected to mutation analysis of the *p53* gene. In the mutation analysis, exon 8 was amplified by PCR as previously described (12), and direct sequencing was performed using the reverse primer and an ABI PRISM 310 Genetic Analyzer (Applied Biosystems, Foster City, CA).

For methylation analysis of the *MLH1* promoter, endometrial scraping cells from 6 patients with endometrial cancers were used to create cell suspensions, which were then each divided into 2 tubes. As described above, cells in one tube were incubated with OBP-401, followed by GFP-based sorting, while the other tube was used as a control. Genomic DNA was extracted from the cells in both tubes. The genomic DNA was modified with sodium bisulfite using a CpGenome DNA Modification Kit (Invitrogen), and was PCR-amplified using methylation-specific primers. The PCR product was subjected to electrophoresis to visualize methylated and unmethylated products, as previously described (13).

Results

Optimizing OBP-401 infection to visualize cancer cells in cytological samples. To effectively visualize cancer cells in cytological samples by GFP fluorescence, it is essential to optimize the conditions of OPB-401 infection, including the

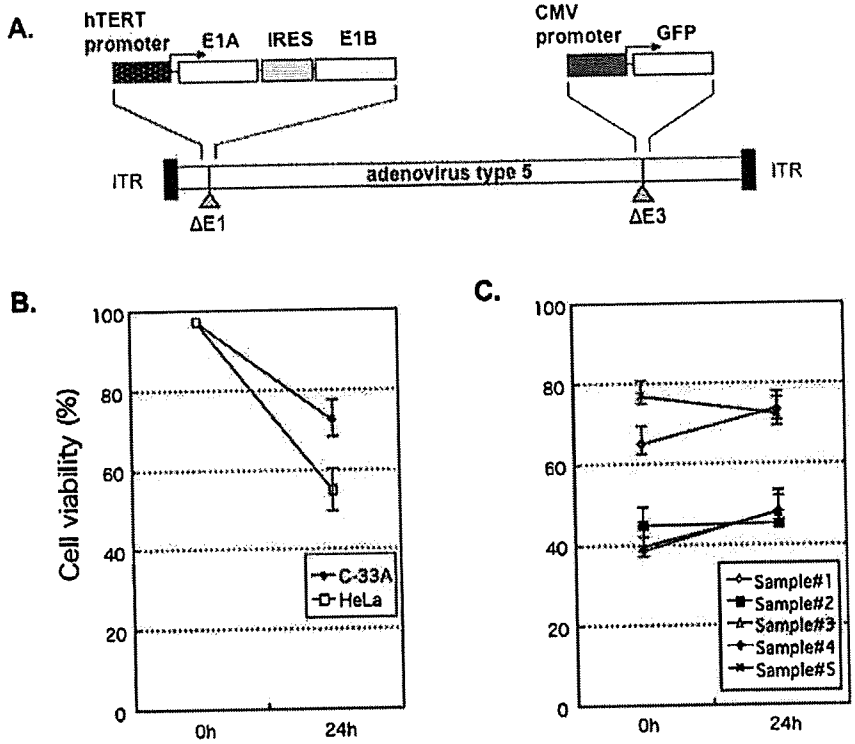

Figure 1. (A) DNA structure of OBP-401. OBP-401 contains the *hTERT* promoter sequence, inserted into the *E3*-deleted adenovirus genome, to drive transcription of the *E1A* and *E1B* bicistronic cassette linked by the internal ribosome entry site structure (IRES), and also contains *GFP* cDNA driven by the cytomegalovirus (*CMV*) promoter. (B and C) Change in viability of suspended cells in culture medium. Cervical cancer cell lines (B) and cervical scraping cells from healthy control patients (C) were suspended in DMEM containing 10% FBS. Cellular viability was evaluated by trypan blue staining before and after incubation for 24 h in the medium. Each point represents the mean ± SD of 3 independent determinants.

time-course of GFP fluoresence, the dose of infection and the viability of cells before and after infection. We first observed the time course of GFP expression. When C33A, HeLa and BJ cells were incubated with OBP-401 at MOIs of 0.01-10 for 24 h, >50% of C33A and HeLa cells incubated at MOIs of >0.1 exhibited significant GFP expression, whereas BJ cells exhibited no GFP expression, even when incubated at MOIs of >10. C33A and HeLa cells began to die between 24 and 48 h after the beginning of incubation, due to the cytotoxic effect of OBP-401, and all C33A and HeLa cells were dead 72 h after the beginning of incubation (data not shown). These results indicate that the optimal time to observe GFP expression is 24 h after the beginning of incubation.

Because gynecologic malignancies are solid tumors, cytological samples must be converted into cell suspensions in medium before infection with OBP-401. The viability of the suspended cells is an important factor, because the cells must survive until at least 24 h after the beginning of incubation, which is the optimal time to observe GFP fluorescence, as described above. We therefore monitored the viability of suspended cells. Cervical exfoliated cells were suspended in DMEM containing 10% FBS, and cellular viability was evaluated by trypan blue staining (Fig. 1B and C). Approximately 40-80% of the cells were found to be viable at the time of sample collection, and their viability did not change during the next 24 h; however, their viability began to decrease 24 h after sample collection. Thus, suspended cells should be used within the first 24 h after sample collection.

Finally, we optimized the dose of OBP-401 for infection of suspended cells. Cervical cancer C33A cells have the highest telomerase activity among cancer cell lines, whereas HeLa cells have relatively low activity. C33A and HeLa cells were suspended in medium, and were then incubated with OBP-401 at various MOIs. For C33A cells, incubation with OBP-401 at 1 MOI was sufficient to obtain significant GFP expression in >90% of cells, whereas HeLa cells had to be incubated with OBP-401 at 10 MOI to obtain the equivalent level of GFP expression (Fig. 2A). Based on these results, we concluded that 10 MOI is the optimal dose of OBP-401 for infection of suspended cells.

Application of OBP-401 system to cancer screening. We then tested the sensitivity of the OBP-401 system for detection of cancer cells *in vitro*. C33A cells were marked by pre-staining with CellTracker Blue, and were then mixed with normal cervical scraping cells at ratios ranging from 1:1 to 1:100000. The total number of cells examined was fixed at $2x10^5$ for each sample, based on the results of preparatory experiments in which we counted the mean number of cells contained in typical cervical scrapings at regular cancer screenings. After these mixed cells were incubated with OBP-401 at 10 MOI for 24 h, we counted the numbers of pre-staining blue signals and GFP-derived green signals. Overall, in each field, almost all cells with blue signals also displayed green signals, whereas none of the cells without blue signals displayed green signals (Fig. 2B). We were able to detect specific green signals on

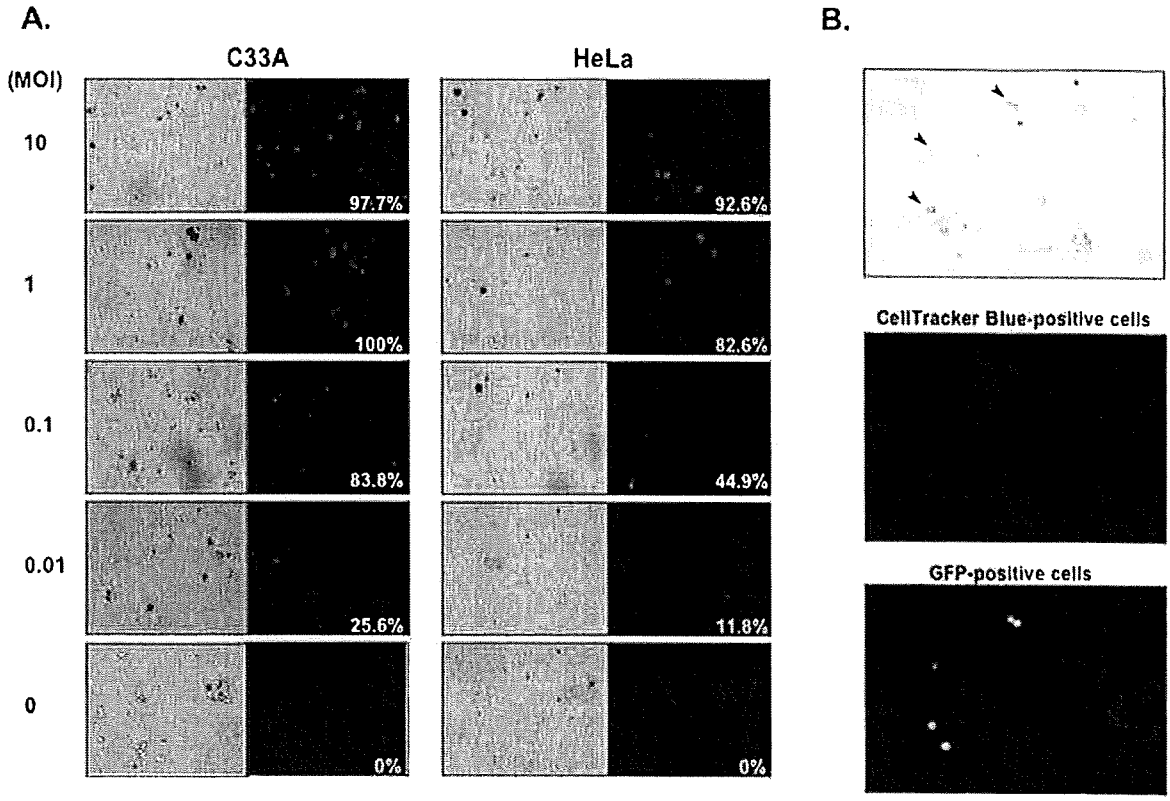

Figure 2. (A) GFP expression in cervical cancer cell lines infected with OBP-401 at various MOIs. Suspensions of cervical cancer cell lines were incubated with OBP-401 at various MOIs, and the ratio of GFP-positive cells was calculated 24 h after the beginning of incubation. (B) Specific visualization of cancer cells via GFP expression. C33A cells were pre-stained with CellTracker Blue and mixed with normal cervical scraping cells. After OBP-401 infection, GFP expression was observed under fluorescence microscopy. (Left) Under light microscopy, C33A cells mixed with normal cervical epithelial cells are recognizable by their specific small, round shapes (arrowhead). (Middle) CellTracker Blue staining clearly distinguishes C33A cells from normal scraping cells. (Right) All CellTracker Blue-stained cells were GFP-positive, indicating that OBP-401-based GFP expression has greater sensitivity and specificity than the CellTracker Blue system for detection of cervical cancer cells.

Table I. Detection of cancer cells in normal cervical scrapings by OBP-401.

C33A ratio	0	1/100000	1/10000	1/1000	1/100	1/10	1
CellTracker-positive cells	0	0	1	3	8	29[b]	123[b]
GFP-positive cells	0	0	1	2	7	26[b]	115[b]
GFP-positive ratio[a]	-	-	100%	66.7%	87.5%	89.7%	93.5%

[a]Percentage of GFP-positive cells in CellTracker-positive cells. [b]Number of cells in randomly selected 10 high power fields.

C33A cells at ratios as high as 1/10000, but at lower ratios we were unable to detect CellTracker Blue-positive or GFP-positive cells (Table I). Thus, it appears that the OBP-401 system detects cancer cells in cytological samples with satisfactory sensitivity.

Next, we attempted to detect cancer cells in clinical scraping samples from 32 patients with histologically confirmed gynecologic cancers (15 cervical cancers, 14 endometrial cancers, 2 vaginal stump cancers and 1 ovarian cancer) and 29 normal control patients. Exfoliated cells including one ascites samples were obtained and the half were subjected to Papanicolau smear testing in which all 32 cancer patients exhibited class V, suggestive of cancer while 29 normal control patients showed class I or II, and the remaining half were suspended in medium and incubated with OBP-401. In samples from 31 of the 32 cancer patients, 24 h after the beginning of incubation, we observed significant GFP expression under fluorescence microscopy, mainly in clusters of atypical cells but also in surrounding solitary cells (Fig. 3), indicating that the sensitivity of the OBP-401 system is extremely high (96%). In contrast, most of the normal cervical samples did not exhibit clear GFP signals (Fig. 3A). However, some normal cervical samples contained single cells with weak GFP expression; those cells had common characteristics

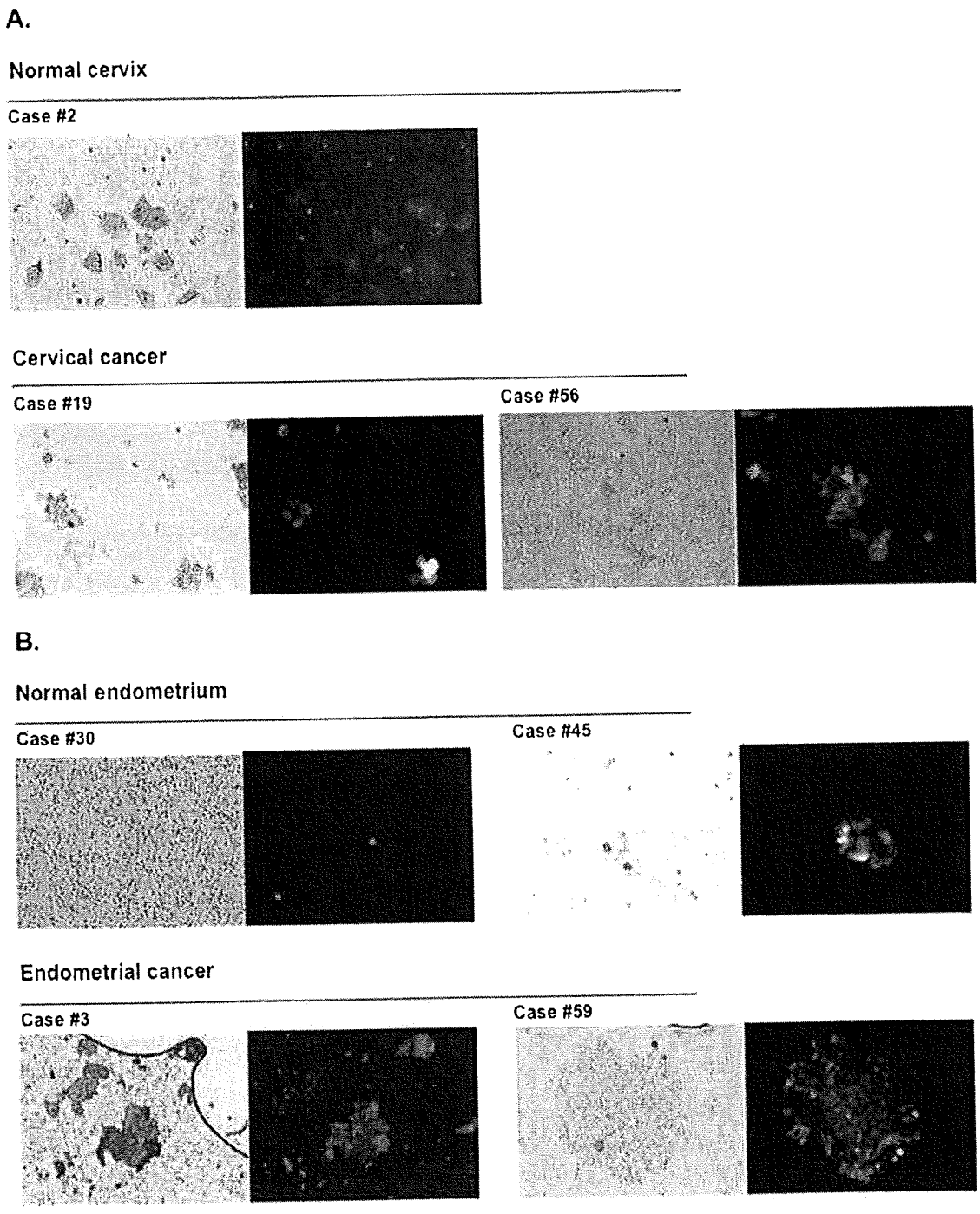

Figure 3. Application of OBP-401 system to visualization of uterine cancer cells in cytological samples. Uterine cervical (A) or endometrial (B) scraping cells from normal controls and cancer patients were incubated with OBP-401 at 10 MOI for 24 h, and were then observed under light microscopy (left), and under fluorescent microscopy for GFP-positive cells (right). Whereas normal cervical samples (case no. 2) exhibited no GFP signals, clear GFP expression was observed in cell clusters from cervical cancer patients. Whereas endometrial cancer samples (case nos. 3 and 59) showed strong GFP expression in atypical cell clusters, some normal endometrial samples (case nos. 0 and 45) exhibited isolated or clustered GFP signals. Original magnification x40 (case no. 3), x100 (case nos. 2 and 59) and x200 (all other cases).

(round shape, small size (diameter ~10 μm) and solitary distribution) that were quite different from those of GFP-positive cells found in cervical cancer specimens. Morphologically, they appeared to be inflammatory cells, mainly neutrophils. Similarly, some normal endometrial scraping samples also contained GFP-positive cells (Fig. 3B), at a higher frequency than normal cervical scrapings. Careful morphological examination revealed that such cells sometimes formed clusters and appeared to be of epithelial origin. We previously reported that normal endometrial epithelial cells

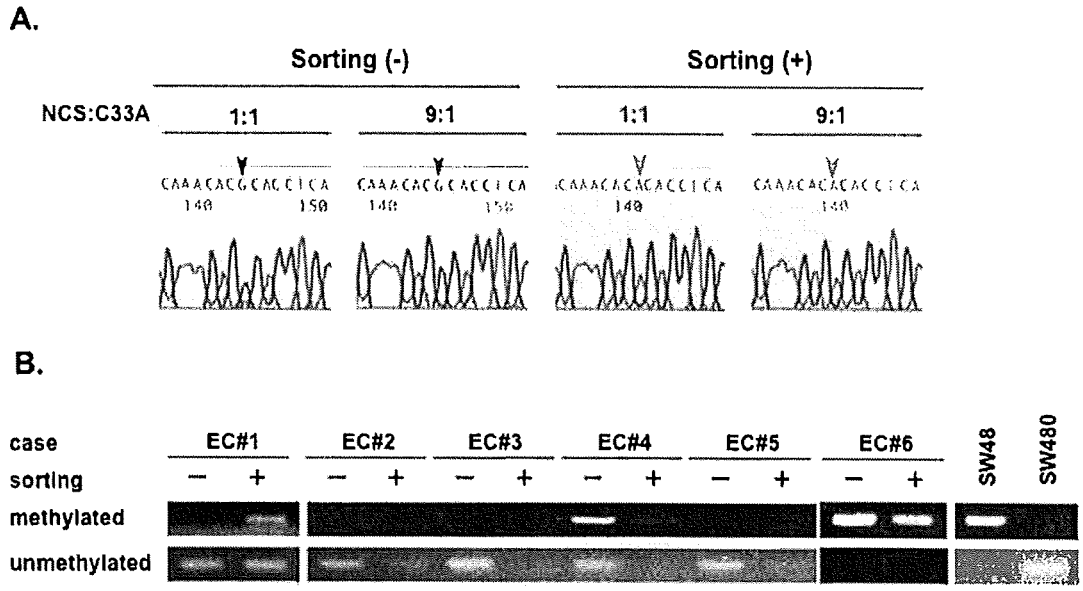

Figure 4. Successful enrichment of cancer cells by sorting of GFP-positive cells. (A) C33A cells were mixed with normal cervical scraping cells (NCS). The ratio of C33A cells was adjusted to 50% (1:1) or 10% (9:1), in a total of $4x10^5$ cells per sample. Half of the mixture was then incubated with OBP-401 for 24 h, followed by sorting of GFP-positive cells. Genomic DNA was extracted from the sorted GFP-positive cells and the uninfected cells, and *p53* mutational analysis was performed by direct sequencing. Arrowheads show the mutation site at codon 273 in exon 8 of the *p53* gene (the wild-type base is guanine). FACS of GFP-positive cells increased the sensitivity of detection of the *p53* mutation in C33A cells mixed with normal scraping cells. (B) Representative results of methylation-specific PCR for *MLH1* promoter using paired endometrial scrapings from 6 patients with endometrial cancers. In each case, one of each pair of samples was infected with OBP-401, followed by sorting of the GFP-positive cells. In 1 cancer case (EC#1), methylated bands were only observed after sorting. In all cancer cases except one (EC#1), unmethylated bands disappeared after sorting, indicating successful enrichment of cancer cells in endometrial scraping samples. Colon cancer SW48 and SW480 cells (which have methylated and unmethylated *MLH1* promoters, respectively) were used as controls.

in the proliferative phase exhibit telomerase activity (14,15). Such activity may be the source of the GFP-positive cells in some of the present normal scraping samples.

OBP-401-based enrichment of cancer cells for genetic analysis. Because OBP-401 infection enabled us to visualize cancer cells with extremely high sensitivity, we attempted to concentrate cancer cells from scraping samples by sorting GFP-positive cells. We first tested the efficacy of such cancer cell enrichment using cancer cell lines. C33A cells, which have a *p53* mutation at codon 273 in exon 8 (CGT ·TGT) (16), were mixed with cervical scraping cells from normal control patients at various ratios. Each of these mixtures was divided into 2 samples, one for infection and the other for non-infection (control); the infection sample was GFP-sorted after 24 h of incubation with OBP-401. Genomic DNA was then extracted from each pair of samples, followed by p53 mutation analysis by direct sequencing. When normal cells were predominant in samples, the *p53* mutation could only be detected after sorting, in the GFP-positive fraction; i.e., the non-sorted samples exhibited wild-type *p53* sequences (Fig. 4A). As the ratio of C33A cells increased, small waves indicating mutated sequences were observed in non-sorted samples, but the waves indicating wild-type sequences remained predominant. These findings indicate that sorting of OBP-401-infected GFP-positive cells is a highly sensitive method of detecting genetic mutations in scraping samples.

We also applied the present GFP-based sorting system to endometrial scrapings. Recent studies indicate that one of the most frequent abnormalities in endometrial carcinogenesis is inactivation of mismatch repair genes, mainly the *MLH1* gene (13,17,18). In 30-40% of endometrial cancers, the *MLH1* promoter region is hypermethylated, leading to silencing of the *MLH1* gene, whereas hypermethylation of the *MLH1* promoter region is extremely rare in normal endometrium. Therefore, we selected *MLH1* hypermethylation as a molecular target for screening of endometrial cancer cells. Endometrial scraping samples from 6 endometrial cancer patients and 6 normal control patients were GFP-sorted after OBP-401 infection. The methylation status of the *MLH1* promoter was then analyzed by methylation-specific PCR. In all normal control samples, the *MLH1* promoter bands were unmethylated (data not shown). However, 2 of the 6 cancer patients (EC#4 and EC#6) had methylated *MLH1* promoter bands in both their sorted GFP-positive fraction and non-sorted samples (Fig. 4B). Interestingly, in 1 cancer case (EC#1), a methylated *MLH1* promoter band was observed in the sorted GFP-positive fraction but not in the non-sorted sample. Furthermore, with the exception of 1 case (EC#1), unmethylated *MLH1* promoter bands observed in the cancer samples before sorting completely disappeared after sorting, indicating that contaminating stromal cells causing generation of unmethylated bands were efficiently eliminated by the sorting of GFP-positive cells. These findings indicate that OBP401 is useful for enriching endometrial cancer cells in scraping samples.

Discussion

The present OBP-401-based screening system is a unique method of detecting cancer cells using telomerase activity as a target, based on consistent reports of studies in which telomerase activation was observed in >90% of cancers, irrespective of tumor type (19,20). A technical advantage of this OBP-401 system is that the GFP signals can be amplified by autonomous viral replication (a useful characteristic of replication-competent adnoviruses), possibly leading to superior sensitivity in detection of cancer cells. In the present study, we identified GFP-positive cancer cells in scraping samples from various gynecologic cancers with extremely high sensitivity (>95%). An additional technical advantage of this system is that cancer cells (even a single cell) can be automatically detected by GFP fluorescence without special knowledge of their morphology; this could be advantageous in hospitals or institutes where conventional cytological screening is not available. Although the present findings indicate that the OBP-401 system has superior sensitivity for detection of cancer cells, it is unclear whether it has superior specificity. In some of the present cervical cancer scraping samples, we detected weak GFP signals that were usually small and isolated. Careful morphological evaluation revealed that those signals were mainly produced by inflammatory cells, especially neutrocytes. In the present study, GFP signals were detected more frequently in normal endometrial samples than in normal cervical samples; we speculate that this is due to constitutive telomerase activity in normal endometrial epithelial cells (14,15). Although the signal intensity of these GFP-positive cells was generally weak, these signals probably decrease the specificity of this system. To overcome these problems, we are currently developing flow cytometry-based quantitative analysis of GFP signaling combined with morphological analysis of single GFP-positive cells, which we expect will greatly improve the specificity of screening.

The present findings indicate that GFP-based sorting after OBP-401 infection is a promising method of enriching cancer cells. In the present *in vitro* analysis in which C33A cells were mixed with normal cervical scraping cells, the *p53* mutation was only detected in GFP-sorted samples, even when normal cervical scraping cells were predominant. In the present experiments using endometrial scraping samples from 6 endometrial cancer patients, 1 patient had methylated *MLH1* promoter bands only in the sorted GFP-positive fraction. Furthermore, most of the endometrial cancer patients exhibited loss of unmethylated bands after sorting, indicating that contaminating stromal cells were effectively eliminated by the sorting. A further advantage of this system is that its sensitivity for detection of genetic abnormalities can be improved by increasing the number of cells subjected to sorting, by scraping as many cells as possible during sampling at cancer screening.

We wish to emphasize that the OBP-401 system can be used to detect a variety of molecular targets. For screening of cervical cancers, the human papillomavirus (HPV) would be a good target. Although detection of HPV by PCR can be sensitive even when crude scraping samples are used (21,22), the OBP-401 system has the advantage of being able to concentrate HPV-positive cancer cells, even when the sample contains a very small number of cervical cancer cells or dysplastic cells. For screening of endometrial cancer, the potential targets include *PTEN*, *KRAS* and *p53* (23). Obviously, the OBP-401 system can also be used to screen other types of cancers. We are currently experimenting with using the OBP-401 system to detect genetic mutations in blood or sputum samples from patients with leukemia or lung cancer, respectively.

In conclusion, we used a telomerase-specific replication-selective adenovirus containing the *GFP* gene to detect cells of various gynecologic cancers. After cell suspensions obtained from cytological samples were incubated for 24 h with OBP-401, fluorescence microscopy revealed strong GFP signals in cancer cells. Although the sensitivity to screen cancer cells appears to be sufficient, the specificity of this system was unsatisfactory, generating GFP signals even in normal endometrial scraping samples, possibly due to the constitutive expression of telomerase activity in endometrial glandular cells. In turn, sorting of GFP-positive cells resulted in successful enrichment of cancer cells, elimination of contaminating stromal components and efficient detection of genetic or epigenetic abnormality in subsequent specific analyses. To further improve the diagnostic accuracy of this system, we are currently studying ways to reduce or distinguish non-specific signals observed in some normal scraping samples.

Acknowledgments

We wish to thank Mr. H. Kawamura, Oncolys BioPharma, Inc., for his helpful information on OBP-401. This study was supported by a Grant-in-Aid for Scientific Research from the Japan Society for the Promotion of Science (JSPS) and the Megumi Medical Foundation of Kanazawa University.

References

1. Mocellin S, Keilholz U, Rossi CR, *et al*: Circulating tumor cells: the 'leukemic phase' of solid cancers. Trends Mol Med 12: 130-139, 2006.
2. Ulmer A, Schmidt-Kittler O, Fischer J, *et al*: Immunomagnetic enrichment, genomic characterization, and prognostic impact of circulating melanoma cells. Clin Cancer Res 10: 531-537, 2004.
3. Ring A, Smith IE and Dowsett M: Circulating tumour cells in breast cancer. Lancet Oncol 5: 79-88, 2004.
4. Cristofanilli M, Budd GT, Ellis MJ, *et al*: Circulating tumor cells, disease progression, and survival in metastatic breast cancer. N Engl J Med 351: 781-791, 2004.
5. Moreno JG, Miller MC, Gross S, *et al*: Circulating tumor cells predict survival in patients with metastatic prostate cancer. Urology 65: 713-718, 2005.
6. Kawashima T, Kagawa S, Kobayashi N, *et al*: Telomerase-specific replication-selective virotherapy for human cancer. Clin Cancer Res 10: 285-292, 2004.
7. Meyerson M, Counter CM, Eaton EN, *et al*: hEST2, the putative human telomerase catalytic subunit gene, is up-regulated in tumor cells and during immortalization. Cell 90: 785-795, 1997.
8. Nakamura TM, Morin GB, Chapman KB, *et al*: Telomerase catalytic subunit homologs from fission yeast and human. Science 277: 955-959, 1997.
9. Takakura M, Kyo S, Kanaya T, *et al*: Cloning of human telomerase reverse transcriptase gene promoter and identification of proximal core promoter essential for transcriptional activation in immortalized and cancer cells. Cancer Res 59: 551-557, 1999.

10. Umeoka T, Kawashima T, Kagawa S, Teraishi F, Taki M, Nishizaki M, Kyo S, Nagai K, Urata Y, Tanaka N and Fujiwara T: Visualization of intrathoracically disseminated solid tumors in mice with optical imaging by telomerase-specific amplification of a transferred green fluorescent protein gene. Cancer Res 64: 6259-6265, 2004.
11. Kishimoto H, Kojima T, Watanabe Y, *et al*: *In vivo* imaging of lymph node metastasis with telomerase-specific replication-selective adenovirus. Nat Med 12: 1213-1219, 2006.
12. Gruszka-Westwood AM, Hamoudi RA, Matutes E, *et al*: p53 abnormalities in splenic lymphoma with villous lymphocytes. Blood 97: 3552-3558, 2001.
13. Kanaya T, Kyo S, Maida Y, *et al*: Frequent hypermethylation of MLH1 promoter in normal endometrium of patients with endometrial cancers. Oncogene 22: 2352-2360, 2003.
14. Kyo S, Takakura M, Kohama T, *et al*: Telomerase activity in human endometrium. Cancer Res 57: 610-614, 1997.
15. Maida Y, Kyo S, Kanaya T, *et al*: Is the telomerase assay useful for screening of endometrial lesions? Int J Cancer 100: 714-718, 2002.
16. Crook T, Wrede D and Vousden KH: p53 point mutation in HPV negative human cervical carcinoma cell lines. Oncogene 6: 873-875, 1991.
17. Esteller M, Levine R, Baylin SB, *et al*: MLH1 promoter hypermethylation is associated with the microsatellite instability phenotype in sporadic endometrial carcinomas. Oncogene 17: 2413-2417, 1998.
18. Simpkins SB, Bocker T, Swisher EM, *et al*: MLH1 promoter methylation and gene silencing is the primary cause of microsatellite instability in sporadic endometrial cancers. Hum Mol Genet 8: 661-666, 1999.
19. Kim NW, Piatyszek MA, Prowse KR, *et al*: Specific association of human telomerase activity with immortal cells and cancer. Science 266: 2011-2015, 1994.
20. Shay JW and Bacchetti S: A survey of telomerase activity in human cancer. Eur J Cancer 33: 787-791, 1997.
21. Franco EL: Primary screening of cervical cancer with human papillomavirus tests. J Natl Cancer Inst Monogr 31: 89-96, 2003.
22. Solomon D: Role of triage testing in cervical cancer screening. J Natl Cancer Inst Monogr 31: 97-101, 2003.
23. Inoue M: Current molecular aspects of the carcinogenesis of the uterine endometrium. Int J Gynecol Cancer 11: 339-348, 2001.

In vivo internal tumor illumination by telomerase-dependent adenoviral GFP for precise surgical navigation

Hiroyuki Kishimoto[a,b,c], Ming Zhao[a], Katsuhiro Hayashi[a,b], Yasuo Urata[d], Noriaki Tanaka[c], Toshiyoshi Fujiwara[c,e], Sheldon Penman[f,1], and Robert M. Hoffman[a,b,1]

[a]AntiCancer, Inc., San Diego, CA 92111; [b]Department of Surgery, University of California, San Diego, CA 92103-8220; [c]Division of Surgical Oncology, Department of Surgery, Okayama University Graduate School of Medicine, Dentistry and Pharmaceutical Sciences, Okayama 700-8558, Japan; [d]Oncolys BioPharma, Inc., Tokyo 106-0032, Japan; [e]Center for Gene and Cell Therapy, Okayama University Hospital, Okayama 700-8558, Japan; and [f]Department of Biology, Massachusetts Institute of Technology, Cambridge, MA 02139-4307

Contributed by Sheldon Penman, June 8, 2009 (sent for review May 10, 2009)

Cancer surgery requires the complete and precise identification of malignant tissue margins including the smallest disseminated lesions. Internal green fluorescent protein (GFP) fluorescence can intensely illuminate even single cells but requires *GFP* sequence transcription within the cell. Introducing and selectively activating the *GFP* gene in malignant tissue in vivo is made possible by the development of OBP-401, a telomerase-dependent, replication-competent adenovirus expressing GFP. This potentially powerful adjunct to surgical navigation was demonstrated in 2 nude mouse models that represent difficult surgical challenges—the resection of widely disseminated cancer. HCT-116, a model of intraperitoneal disseminated human colon cancer, was labeled by virus injection into the peritoneal cavity. A549, a model of pleural dissemination of human lung cancer, was labeled by virus administered into the pleural cavity. Only the malignant tissue fluoresced brightly in both models. In the intraperitoneal model of disseminated cancer, fluorescence-guided surgery enabled resection of all tumor nodules labeled with GFP by OBP-401. The data in this report suggest that adenoviral-GFP labeling tumors in patients can enable fluorescence-guided surgical navigation.

Adenovirus | green fluorescent protein | metastasis

The intent of cancer surgery is to remove malignant tissue together with margins of presumably normal tissue (1–3) to ensure complete removal of abnormal cells. Estimating margin width during surgery is critical and depends on the surgeon's vision. There have been many developments intended to improve the delineation of tissue margins using morphologic and optical differences between normal and abnormal tissue. This report describes a major enhancement of cancer surgical navigation using the selective fluorescent labeling, in vivo, of malignant tissue. Bright GFP fluorescence clearly illuminates the tumor boundaries and facilitates detection of the smallest disseminated disease lesions.

Highly selective viral replication in malignant cells growing in normal tissue has recently become possible using novel adenoviruses, OBP-301 (4–6) and, more recently, OBP-401 (7, 8). This latter virus, which can enter most cells, contains the replication cassette with the human telomerase reverse transcriptase (hTERT) promoter driving the expression of the viral *E1* genes, and the inserted *GFP* gene. Virus replication and, hence, *GFP* gene expression occur only in the presence of an active telomerase, i.e., in malignant tissue (7). The OBP-401 virus was first tested by injection directly into HT-29 human colon tumors orthotopically implanted into the rectum in BALB/c *nu/nu* mice (7). Subsequent para-aortic lymph node metastasis was observed by laparotomy under fluorescence. The adaption of GFP fluorescence to in vivo labeling of tumor tissue should facilitate precision surgical navigation in live animals and, very possibly, in a clinical surgical setting.

Results

Fluorescence Labeling of Human Cancer Cells with OBP-401 in Vitro. A549 tumor cells, growing in tissue culture, were infected with OPP-401, and the development of GFP fluorescence followed. The fluorescence intensity gradually increased after infection as the virus, with its *GFP* gene, replicated (Fig. 1*A*).

The extent of infection was tested by infecting red fluorescent protein (RFP)-expressing cancer cells, growing in cell culture, with OBP-401. These included A549-RFP, PC-3-RFP, HCT-116-RFP, and HT-29-RFP cells. In most cells, the introduction of green fluorescence changes the cell color from red to yellow, showing that most were infected by OBP-401. Any remaining red fluorescence clearly identifies those few cells that remain uninfected by the adenovirus. The color changes increased gradually followed by cell death due to the cytopathic effect of replicating OBP-401 (Fig. 1 *B* and *C*).

Fluorescence Labeling of Subcutaneous Tumors by Infection in Vivo with OBP-401. Both nonfluorescent PC-3 and red fluorescent PC-3-RFP human prostate cancer cells were inoculated s.c. (Fig. 2 *A* and *B*). The resulting s.c. tumors were injected with 1×10^8 plaque-forming units (PFU) of OBP-401 as shown in Fig. 2*B*. A color change from red to yellow in the s.c. PC-3-RFP tumor and the onset of GFP fluorescence in the nonfluorescent PC-3 tumor were observed by the third day after virus injection (Fig. 2*C*). An RFP filter selectively showed the tumors' endogenous RFP fluorescence (Fig. 2*D*). Similarly, a GFP filter showed GFP fluorescence induced in the tumors by OBP-401 (Fig. 2*E*). Infecting tumor cells that are endogenously expressing RFP with the GFP-expressing adenoviral vector OBP-401 clearly shows the extent of GFP labeling of the tumor. Cells showing a yellow fluorescence are infected with OBP-401, while the remaining red fluorescent cells clearly indicate the small portion that might remain uninfected.

Labeling Peritoneal Carcinomatosis with OBP-401. Peritoneal carcinomatosis was induced in the abdominal cavity of nude mice by inoculating 3×10^6 red fluorescent HCT-116-RFP human colorectal cancer cells. Various sized peritoneal disseminated nodules developed within 12 days. These were clearly visible by fluorescence imaging using a long-pass filter and/or a specific RFP filter (Fig. 3 *A* and *B*). Even very small disseminated nodules were illuminated by RFP fluorescence (Fig. 3*B*). Although there was some autofluorescence from adjacent organs visible, the tumor nodules were not visible through a GFP filter (Fig. 3 *A* and *B*).

Author contributions: H.K., Y.U., N.T., T.F., and R.M.H. designed research; H.K., M.Z., and K.H. performed research; H.K., Y.U., N.T., T.F., S.P., and R.M.H. analyzed data; and H.K., S.P., and R.M.H. wrote the paper.

The authors declare no conflict of interest.

[1]To whom correspondence may be addressed. E-mail: penman@mit.edu or all@anticancer.com.

www.pnas.org/cgi/doi/10.1073/pnas.0906388106

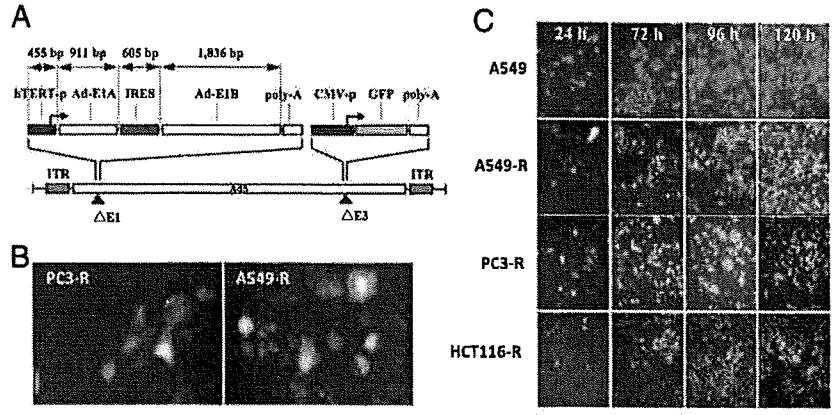

Fig. 1. Structure of OBP-401, virus replication in human cancer cells and induced GFP expression. (*A*) Schematic DNA structure of OBP-401. OBP-401 is a telomerase-specific replication-competent adenovirus variant, in which the hTERT promoter element drives the expression of *E1A* and *E1B* genes linked with an IRES. The *GFP* gene is inserted under the CMV promoter into the E3 region. (*B*) A549-RFP and PC-3-RFP cells changed color after infection with OBP-401 at a multiplicity of injection (MOI) of 10. (Magnification, 200×.) (*C*) Noncolored A549 as well as RFP-expressing cancer cells A549-RFP, PC-3-RFP, and HCT-116-RFP were infected with OBP-401 at an MOI of 10. Cells were assessed at indicated time points for GFP expression under fluorescence microscopy. After OBP-401 infection, noncolored A549 cells expressed GFP fluorescence. In A549-RFP, PC-3-RFP, and HCT-116-RFP, color changes from red to yellow were detected. The color changes increased gradually in a time-dependent fashion. (Magnification, 200×.)

Once the malignant nodules were established at 12 days after intraperitoneal (i.p.) implantation of HCT-116-RFP cells, 1×10^8 PFU OBP-401 were injected into the mouse abdominal cavity. Selective color filters showed that the HCT-116-RFP disseminated nodules expressed GFP fluorescence as well as RFP when examined 5 days later (Fig. 3*C*). RFP fluorescence

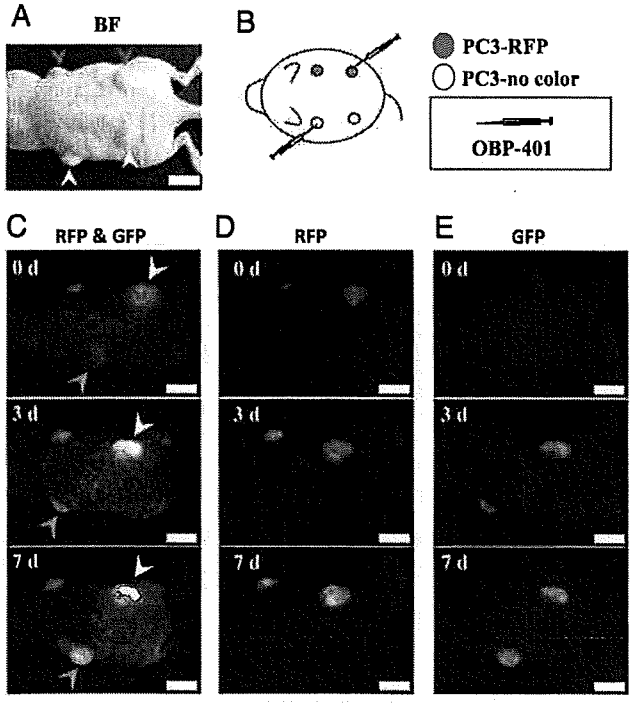

Fig. 2. Selective visualization of s.c. tumors in vivo after OBP-401 GFP-labeling. s.c. tumors of noncolored PC-3 (*A*, white arrowheads) or PC-3-RFP (*A*, red arrowheads) human prostate cancer cells were intratumorally injected with PBS for control or OBP-401 at a dose of 1×10^8 PFU as shown in *B*. After intratumoral injection of OBP-401, GFP fluorescence was detected in noncolored PC-3 s.c. tumors (*C*, green arrowheads) and a color change from red to yellow was also observed in PC-3-RFP tumors by fluorescence imaging using a long-pass filter to simultaneously observe both GFP and RFP (*C*, yellow arrowheads). With specific filters, the tumors endogenous RFP fluorescence (*D*) and GFP fluorescence induced by OBP-401 (*E*) were individually detected. (Scale bar, 10 mm.)

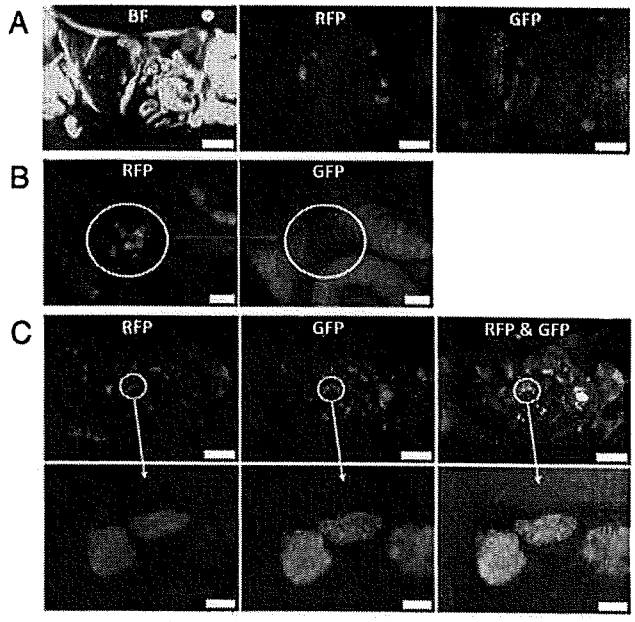

Fig. 3. Intraperitoneal injection of OBP-401 visualized peritoneal dissemination of HCT-116-RFP cells. (*A*) HCT-116-RFP human colorectal cancer cells were inoculated into the abdominal cavity of nude mice. Various sized disseminated peritoneal nodules appeared within 12 days. (Scale bar, 10 mm.) (*B*) At higher magnification, peritoneally disseminated nodules of HCT-116-RFP were clearly visible using a specific filter for RFP (*Left*), and these nodules did not express GFP (*Right*). (Scale bar, 2 mm.) (*C*) Mice with HCT-116-RFP peritoneal disseminated nodules were i.p. injected with OBP-401 at a dose of 1×10^8 PFU. Five days after virus administration, HCT-116-RFP peritoneal-disseminated nodules were detected with their endogenous RFP fluorescence (*Left*). These disseminated nodules now expressed GFP fluorescence (*Middle*). With the long-pass filter, for simultaneous observation of both GFP and RFP, it can be seen that all of the RFP tumors were apparently labeled with GFP after OBP-401 injection (*Right*). (Scale bars: *Upper*, 10 mm; *Lower*, 500 μm.)

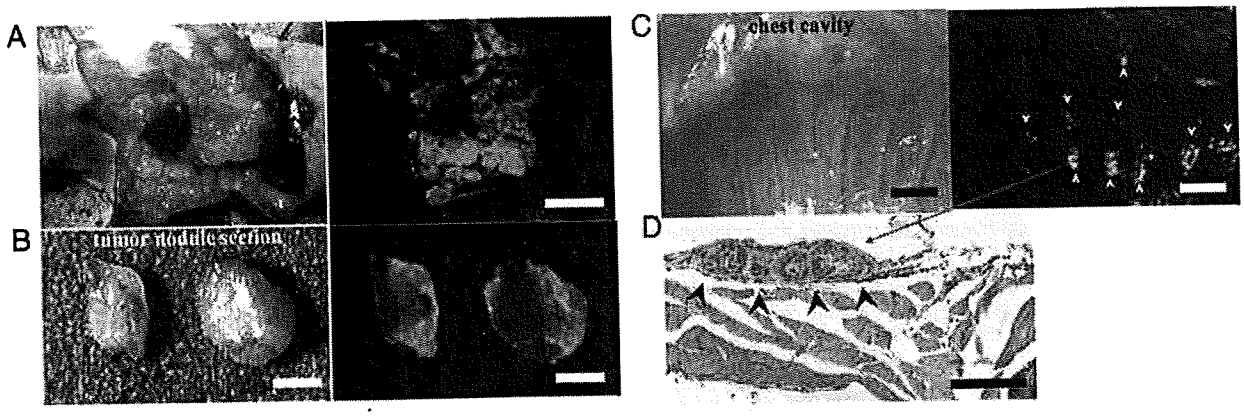

Fig. 4. Intrapleural injection of OBP-401 visualized pleural disseminations of A549 cells. (*A*) Two weeks after implantation of noncolored A549 cells into the thoracic space, OBP-401 at a dose of 1×10^8 PFU, was intrapleurally injected. Five days later, disseminated nodules were visualized by GFP fluorescence (*Right*). (Scale bar, 10 mm.) (*B*) Cross-section of pleural disseminated nodule. GFP expression was seen on the surface of pleurally disseminated nodules (*Right*). (Scale bar, 2 mm.) (*C*) Very small lesions that were not detectable in brightfield were visualized by GFP fluorescence (*Right*, arrowheads). (Scale bar, 2 mm.) (*D*) Histological analysis with H&E confirmed that these GFP-expressing lesions were adenocarcinomas (arrowheads). (Scale bar, 100 μm.)

was essentially coincident with that of GFP (Fig. 3*C*). These results indicate that i.p. injection of OBP-401 efficiently infected and labeled disseminated cancer.

Labeling of Pleurally Disseminated Cancer with OBP-401. These experiments assessed the effectiveness of OBP-401 labeling of pleural carcinomatosis in a mouse model of unlabeled A549 human lung cancer cells. The thoracic space of nude mice was inoculated with 2×10^6 cancer cells. Various sized disseminated plural nodules appeared within 10 days after implantation. At this time, 1×10^8 PFU of OBP-401 were injected into the thoracic cavity. Five days after injection of OBP-401, the cavity was examined using GFP fluorescence imaging. A representative mouse is shown in Fig. 4. Disseminated pleural nodules were visualized by GFP expression (Fig. 4 *A* and *B*). Even very small lesions, which are normally undetectable, were clearly illuminated by GFP fluorescence (Fig. 4*C*). Histological examination confirmed that these GFP-expressing tissues were adenocarcinomas. A representative histological section is shown in Fig. 4*D*. These results suggest that intrapleural injection of at least 1×10^8 PFU of OBP-401 can efficiently label disseminated pleural cancer. Lower doses of OBP-401 resulted in less efficient labeling.

OBP-401 Fluorescence-Guided Resection of Disseminated Peritoneal Tumors. In order to test the effectiveness of OBP-401-guided cytoreduction surgery, we used the peritoneal carcinomatosis model with nonfluorescent HCT-116 human colon cancer cells. Mice with peritoneal carcinomatosis were injected i.p. with OBP-401 at a dose of 1×10^8 PFU. Five days after viral administration, laparotomy was performed to remove intra-abdominal disease using fluorescence-guided navigation under anesthesia (Fig. 5 *A* and *B*). A representative mouse after cytoreduction surgery with OBP-401-navigation is shown in Fig. 5*C*. Disseminated cancer nodules, which would otherwise be undetectable, were clearly visible by bright GFP fluorescence. The resected nodules were visualized as frozen sections under both fluorescence (Fig. 5*D*) and after hematoxylin and eosin (H&E) staining (Fig. 5 *E* and *F*). These results suggest that OBP-401-labeling has significant potential for guiding cytoreduction surgery of disseminated cancer.

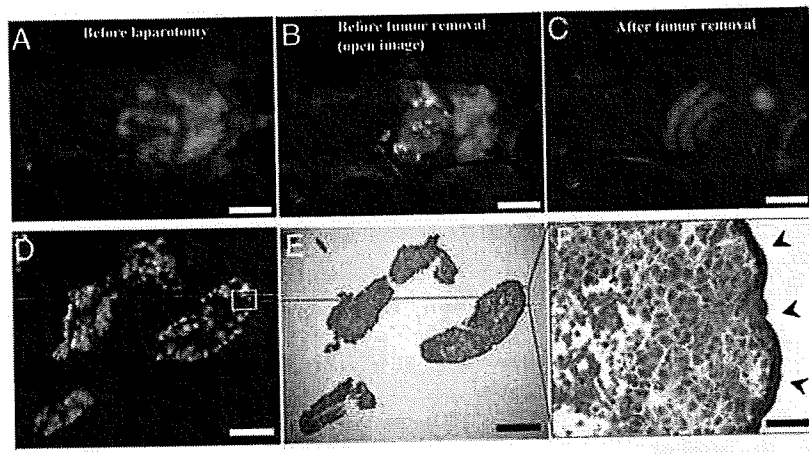

Fig. 5. Fluorescence-guided surgical removal of peritoneal disseminated HCT-116 tumors after GFP labeling with OBP-401. Noncolored HCT-116 human colon cancer cells were injected into the abdominal space of nude mice. Ten days later, 1×10^8 PFU of OBP-401 were i.p. injected. (*A*) Disseminated nodules were efficiently labeled and noninvasively visualized by GFP expression 5 days after virus administration. (*B*) Under general anesthesia, laparotomy was performed to remove intra-abdominal disease under GFP-guided navigation. (*C*) Disseminated nodules visualized by GFP-guided navigation were removed. (Scale bars: *A–C*, 10 mm.) (*D*) Frozen section of resected HCT-116 disseminated nodules with fluorescence detection. (Scale bar, 500 μm.) (*E*) H&E section of HCT-116 disseminated nodules shown in *D*. The box outlines a region of *D* and *E* analyzed in *F*. (Scale bar, 500 μm.) (*F*) Detail of the boxed region of *D* and *E*. (Scale bar, 50 μm.)

Discussion

The peritoneal surface is involved in more than 20% of patients with gastric, colon, and pancreatic cancers (1). Cytoreduction surgery requires resection of all visible tumors and stripping of all peritoneal surfaces that contain metastatic nodules (1, 2, 9). Therefore, visceral peritoneal involvement often requires concomitant resection of intra-abdominal organs such as the small intestine and colorectum.

The detection of small macroscopic peritoneal lesions is largely limited by the weak contrast between tumor nodules and surrounding normal tissues. Technology improving the intraoperative detection of peritoneal disease would facilitate essentially complete cytoreduction in these patients. The photosensitizer, 5-aminolevulinic acid (5-ALA) has been used for intraoperative detection of cancer lesions in neurosurgery (10). However, labeling that is essentially cancer-selective can be a powerful surgical adjunct. This report shows that OBP-401 infection of cancer cells leads to the highly selective induction of bright GFP fluorescence.

Implanting RFP-expressing cancer cell lines gave rise to fluorescent nodules whose color change clearly indicated the efficiency with which OBP-401 labeled disseminated peritoneal tumors with GFP. The change from red to yellow fluorescence indicated successful infection by OBP-401 (Fig. 3). Similarly, OBP-401 GFP labeling could detect dissemination nodules with high sensitivity in a pleural carcinomatosis model (Fig. 4).

Perhaps most importantly, we could remove disseminated disease in a peritoneal carcinomatosis model by using fluorescence-guided resection. These results suggest developing a dedicated excitation light for fluorescence-guided surgery similar to that described for use in mice (11). In the present study, during surgery, even very small peritoneal lesions could be identified with GFP fluorescence (11).

Materials and Methods

Recombinant Adenovirus. OBP-401, containing the *GFP* gene under the control of the CMV promoter with the hTERT promoter driving the *E1A* and *E1B* genes, was constructed as previously described (6, 7). OBP-401 was purified by ultracentrifugation in cesium chloride step gradients. Virus titers were determined by a plaque-forming assay using 293 cells. The virus was stored at −80°C.

Cell Culture. The human non-small cell lung cancer cell line A549, the human colorectal cancer cell lines HCT-116 and HT-29, and the human prostate cancer cell line PC-3 were cultured in RPMI 1640 medium supplemented with 10% FBS.

Production of RFP Retroviral Vector. For RFP retrovirus production, the *HindIII/NotI* fragment from pDsRed2 (Clontech), containing the full-length RFP cDNA, was inserted into the *HindIII/NotI* site of pLNCX2 (Clontech) containing the neomycin-resistance gene. PT67, a NIH 3T3-derived packaging cell line (Clontech), expressing the viral envelope, was cultured in DMEM supplemented with 10% FBS. For vector production, PT67 packaging cells, at 70% confluence, were incubated with a precipitated mixture of LipofectAMINE reagent (Life Technologies) and saturating amounts of pLNCX2-DsRed2 plasmid for 18 h. Fresh medium was replenished at this time. The cells were examined by fluorescence microscopy 48 h post-transduction. For selection of a clone producing high amounts of RFP retroviral vector (PT67-DsRed2), the cells were cultured in the presence of 200 to 1,000 μg/mL G418 (Life Technologies) for 7 d. The isolated packaging cell clone was termed PT67-DsRed2 (12–15).

***RFP* Gene Transduction of Cancer Cells.** For *RFP* gene transduction, cancer cells were incubated with a 1:1 precipitated mixture of retroviral supernatants of PT67-DsRed2 cells and RPMI 1640 containing 10% FBS for 72 h. Fresh medium was replenished at this time. Tumor cells were harvested with trypsin/EDTA 72 h post-transduction and subcultured at a ratio of 1:15 into selective medium, which contained 200 μg/mL G418. To select brightly fluorescent cells, the level of G418 was increased up to 800 μg/mL in a stepwise manner. RFP-expressing cancer cells were isolated with cloning cylinders (Bel-Art Products) using trypsin/EDTA. Cells were amplified by conventional culture methods in the absence of selective agent (12–15).

Animal Experiments. Athymic nude mice were kept in a barrier facility under HEPA filtration. Mice were fed with autoclaved laboratory rodent diet (Tecklad LM-485, Western Research Products). All animal studies were conducted in accordance with the principals and procedures outlined in the National Institutes of Health Guide for the Care and Use of Laboratory Animals under assurance A3873-01.

Subcutaneous Tumor Model. Subcutaneous tumors were produced by injection of 3×10^6 noncolored PC-3 or PC-3-RFP human prostate cancer cells in 5-week old nude mice. When tumors reached approximately 6 mm in diameter, the tumors were intratumorally injected with PBS for control or OBP-401 at a dose of 1×10^8 PFU in 100 μL PBS. Mice were examined for fluorescence expression with a long-pass filter (a filter for simultaneous observation of both GFP and RFP) or with specific filters for GFP or RFP.

Peritoneal Carcinomatosis Model of HCT-116 Human Colon Cancer Cells. Five-week-old nude mice were i.p. injected with noncolored HCT-116 or HCT-116-RFP human colon cancer cells (3×10^6 in 200 μL HBSS) using a 27-gauge needle. Twelve days after cancer cell inoculation, mice were injected i.p. with OBP-401 at a dose of 1×10^8 PFU in 200 μL PBS. Five days after virus injection, the abdominal cavity was directly examined by fluorescence imaging under anesthesia.

Pleural Carcinomatosis Model of A549 Human Lung Cancer Cells. Five-week-old nude mice were inoculated with noncolored A549 cells (2×10^6 cells in 200 μL HBSS) into the thoracic space using a 27-gauge needle. Ten days after cancer cell inoculation, OBP-401 at a dose of 1×10^8 PFU in 200 μL PBS was intrapleurally injected. Five days after virus injection, the pleural cavity was directly imaged for GFP expression. GFP-expressing tissues were removed and examined microscopically.

Fluorescence Optical Imaging and Processing. An Olympus OV100 Small Animal Imaging System containing an MT-20 light source was used. High-resolution images were captured directly on a PC (Fujitsu Siemens). Images were analyzed with the use of Cell^R software (Olympus Biosystems) (16).

Histological Examination. For histological studies, GFP-expressing tissues were removed at the time of sacrifice and put into buffered formalin for 24 h at room temperature. All of the tissues were subsequently processed through alcohol dehydration and paraffinization. Tissues were embedded in paraffin and sectioned at 5 μm. All slides were stained by H&E, and examined microscopically.

ACKNOWLEDGMENTS. This project was supported in part by National Cancer Institute Grant CA132242.

1. Sugarbaker PH (2004) Managing the peritoneal surface component of gastrointestinal cancer. Part 1. Patterns of dissemination and treatment options. *Oncology* 18:51–59.
2. Sugarbaker PH (2004) Managing the peritoneal surface component of gastrointestinal cancer. Part 2. Perioperative intraperitoneal chemotherapy. *Oncology* 18:207–219.
3. Glehen O, et al. (2004) Cytoreductive surgery combined with perioperative intraperitoneal chemotherapy for the management of peritoneal carcinomatosis from colorectal cancer: A multi-institutional study. *J Clin Oncol* 22:3284–3292.
4. Kawashima T, et al. (2004) Telomerase-specific replication-selective virotherapy for human cancer. *Clin Cancer Res* 10:285–292.
5. Taki M, et al. (2005) Enhanced oncolysis by a tropism-modified telomerase-specific replication-selective adenoviral agent OBP-405 ('Telomelysin-RGD'). *Oncogene* 24:3130–3140.
6. Umeoka T, et al. (2004) Visualization of intrathoracically disseminated solid tumors in mice with optical imaging by telomerase-specific amplification of a transferred green fluorescent protein gene. *Cancer Res* 64:6259–6265.
7. Kishimoto H, et al. (2006) In vivo imaging of lymph node metastasis with telomerase-specific replication-selective adenovirus. *Nat Med* 12:1213–1219.
8. Fujiwara T, et al. (2006) Enhanced antitumor efficacy of telomerase-selective oncolytic adenoviral agent OBP-401 with docetaxel: Preclinical evaluation of chemovirotherapy. *Int J Cancer* 119:432–440.
9. Sadeghi B, et al. (2000) Peritoneal carcinomatosis from non-gynecologic malignancies: Results of the EVOCAPE 1 multicentric prospective study. *Cancer* 88:358–363.
10. Stepp H, et al. (2007) ALA and malignant glioma: Fluorescence-guided resection and photodynamic treatment. *J Environ Pathol Toxicol Oncol* 26:157–164.
11. Yang M, Luiken G, Baranov E, Hoffman RM (2005) Facile whole-body imaging of internal fluorescent tumors in mice with an LED flashlight. *Biotechniques* 39:170–172.
12. Hoffman RM (2005) The multiple uses of fluorescent proteins to visualize cancer in vivo. *Nat Rev Cancer* 5:796–806.
13. Hoffman RM, Yang M (2006) Subcellular imaging in the live mouse. *Nature Protoc* 1:775–782.
14. Hoffman RM, Yang M (2006) Color-coded fluorescence imaging of tumor-host interactions. *Nature Protoc* 1:928–935.
15. Hoffman RM, Yang M (2006) Whole-body imaging with fluorescent proteins. *Nature Protoc* 1:1429–1438.
16. Yamauchi K, et al. (2006) Development of real-time subcellular dynamic multicolor imaging of cancer-cell trafficking in live mice with a variable-magnification whole-mouse imaging system. *Cancer Res* 66:4208–4214.

A simple biological imaging system for detecting viable human circulating tumor cells

Toru Kojima,[1,2] Yuuri Hashimoto,[1,3] Yuichi Watanabe,[1,3] Shunsuke Kagawa,[1,2] Futoshi Uno,[1,2] Shinji Kuroda,[1,2] Hiroshi Tazawa,[2] Satoru Kyo,[4] Hiroyuki Mizuguchi,[5] Yasuo Urata,[3] Noriaki Tanaka,[1] and Toshiyoshi Fujiwara[1,2]

[1]Division of Surgical Oncology, Department of Surgery, Okayama University Graduate School of Medicine, Dentistry and Pharmaceutical Sciences, Okayama, Japan. [2]Center for Gene and Cell Therapy, Okayama University Hospital, Okayama, Japan. [3]Oncolys BioPharma Inc., Tokyo, Japan. [4]Department of Obstetrics and Gynecology, Kanazawa University School of Medicine, Kanazawa, Japan. [5]Department of Biochemistry and Molecular Biology, Graduate School of Pharmaceutical Sciences, Osaka University, Osaka, Japan.

The presence of circulating tumor cells (CTCs) in the peripheral blood is associated with short survival, making the detection of CTCs clinically useful as a prognostic factor of disease outcome and/or a surrogate marker of treatment response. Recent technical advances in immunocytometric analysis and quantitative real-time PCR have made it possible to detect a few CTCs in the blood; however, there is no sensitive assay to specifically detect viable CTCs. Here, we report what we believe to be a new approach to visually detect live human CTCs among millions of peripheral blood leukocytes, using a telomerase-specific replication-selective adenovirus expressing GFP. First, we constructed a GFP-expressing attenuated adenovirus, in which the telomerase promoter regulates viral replication (OBP-401; TelomeScan). We then used OBP-401 to establish a simple ex vivo method that was able to detect viable human CTCs in the peripheral blood. The detection method involved a 3-step procedure, including the lysis of rbc, the subsequent addition of OBP-401 to the cell pellets, and an automated scan using fluorescence microscopy. OBP-401 infection increased the signal-to-background ratio as a tumor-specific probe, because the fluorescent signal was amplified only in viable, infected human tumor cells, by viral replication. This GFP-expressing virus-based method is remarkably simple and allows precise enumeration of CTCs.

Introduction

Determination of the extent of the disease is the most important factor in predicting the clinical outcome in cancer patients. Primary cancers have been known to shed tumor cells into the blood circulation, which represents the route for systemic tumor cell dissemination (1, 2). Indeed, the presence of circulating tumor cells (CTCs) in the peripheral blood is associated with short survival, and therefore the detection of CTCs is clinically useful as a prognostic factor of disease outcome and/or as a surrogate marker of treatment response (3, 4). Technical advances in immunocytometric analysis and quantitative real-time PCR have made it possible to detect a few CTCs in the blood; however, background expression of cancer-associated antigens, such as cytokeratin 8 (CK-8), CK-18, and CK-19, in normal epithelial cells results in the false-positive detection, and PCR-based methods can not permit analysis of cell morphology. Moreover, there is no sensitive assay for detecting viable CTCs.

The GFP, which was originally identified from the jellyfish *Aequorea victoria*, is an attractive molecular marker for imaging in live tissues because of the relatively noninvasive nature of fluorescent (5–8). It has been reported that hormone-refractory human prostate carcinoma, growing orthotopically in nude mice, efficiently deliver viable tumor cells in the host circulation, which could be detectable using the fluorescence microscopy, when marked by GFP expression (9). In addition, isolated rare CTCs showed an increased metastatic propensity. We reported previously that intratumoral injection of telomerase-specific replication-selective adenovirus expressing the *gfp* gene (OBP-401; TelomeScan) causes viral spread into the regional lymphatics, with subsequent selective replication in neoplastic lesions, resulting in GFP expression in metastatic lymph nodes in *nu/nu* mice (10). The present study extended our previous work, by developing what we believe to be a novel and simple strategy to selectively label human CTCs with fluorescence among millions of peripheral blood leukocytes. The detection method involves 3-steps: the lysis of rbc, the subsequent addition of OBP-401 to the cell pellets, and the automated scan under the fluorescence microscope. This method allows precise enumeration of human CTCs, because OBP-401 can replicate and express GFP fluorescence only in viable tumor cells.

Results

Selective GFP expression in human cancer cells in vitro by OBP-401. OBP-401 (TelomeScan) was constructed by inserting the *gfp* gene under the control of the CMV promoter at the deleted E3 region of the telomerase-specific replication-selective type 5 adenovirus OBP-301 (Telomelysin) (11, 12) (Figure 1). To determine whether telomerase activity is associated with selective GFP expression in different cancer cell lines, we measured human telomerase reverse transcriptase (*hTERT*) mRNA and GFP expression using quantitative real-time RT-PCR analysis and fluorescence microplate reader, respectively. The *hTERT* expression was directly proportional to the fluorescence intensity, and regression analysis confirmed a strong correlation between these numbers ($r^2 > 0.94$) (Figure 1B). H1299 human non–small cell lung cancer cells expressed bright GFP fluorescence as early as 12 hours after OBP-401 infection, and a positive signal for GFP was detected in all cells at 48 hours after infec-

Conflict of interest: Yasuo Urata is an employee of Oncolys BioPharma Inc., the manufacturer of OBP-401 (TelomeScan).

Citation for this article: *J. Clin. Invest.* doi:10.1172/JCI38609.

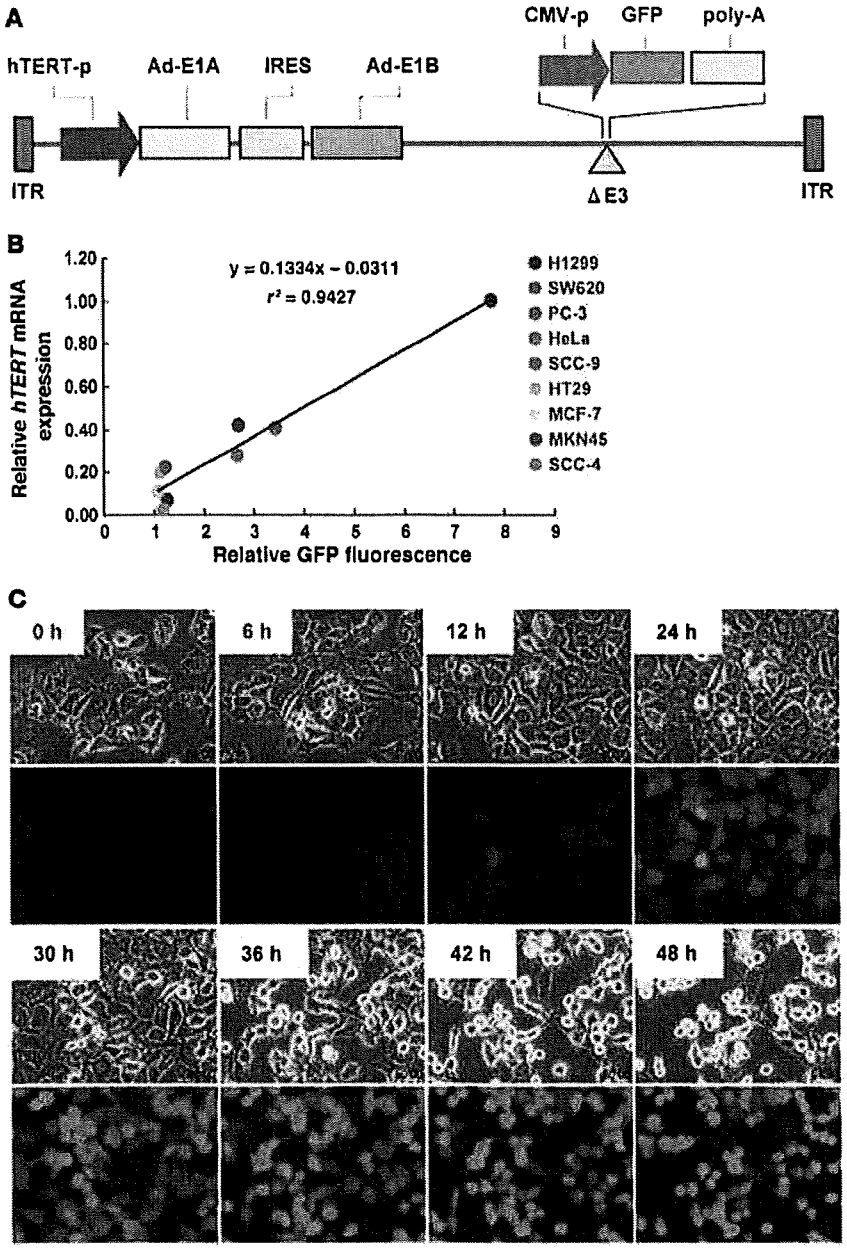

Figure 1
Schematic DNA structure of OBP-401 and selective replication of OBP-401 in human cancer cells. (**A**) OBP-401 is a telomerase-specific replication-competent adenovirus variant, in which the hTERT promoter element drives expression of the *E1A* and *E1B* genes linked with an IRES, and the *gfp* gene is inserted under the CMV promoter into the E3 region for monitoring viral replication. hTERT-p, hTERT promoter; Ad-E1A, adenoviral E1A; Ad-E1B, adenoviral E1B; CMV-p, CMV promoter; poly-A, polyadenylation signal; ITR, inverted terminal repeat. (**B**) Relationship between *hTERT* expression and GFP fluorescence. Relative *hTERT* mRNA expression and GFP fluorescence in human tumor cell lines were determined by real-time RT-PCR analysis and fluorescence microplate reader, respectively. The relative *hTERT* mRNA expression ratios normalized by dividing the value of H1299 cells are presented for each sample. Relative GFP fluorescence was measured 48 hours after OBP-401 infection at an MOI of 10. (**C**) Time-lapse images of H1299 human lung cancer cells were recorded for 48 hours after OBP-401 infection at an MOI of 10. Selected images taken at the indicated time points show cell morphology by phase-contrast microscopy (top panels) and GFP expression under fluorescence microscopy (bottom panels). Original magnification, ×200.

tion (Figure 1C and Supplemental Video 1; supplemental material available online with this article; doi:10.1172/JCI38609DS1). OBP-401 infection also induced GFP expression in other neoplastic cells such as human sarcoma cell lines within 24 hours after infection (Supplemental Figure 1 and Supplemental Video 2). In parallel experiments, OBP-401 infection induced dose-dependent GFP expression in a variety of human cancer cell lines that originated from different organs (Supplemental Figure 2).

Measurement of viable CTCs with OBP-401 in the blood. We used OBP-401 to establish a simple ex vivo method for detecting viable human CTCs in the peripheral blood. As illustrated in Figure 2A, the method involves a 3-step procedure, including the lysis of rbc in 5-ml aliquots of whole blood samples, subsequent addition of 10^4 PFUs of OBP-401 to the cell pellets, and the deposition of cells on polylysine-coated slides, followed by automated scanning under a fluorescence microscope. OBP-401 infection increases the signal-to-background ratio as a tumor-specific probe, because the fluorescent signal can be amplified only in tumor cells by telomerase-specific viral replication. The automated optical scan system provides high speed and accuracy of slide movement in all x, y, and z directions for the acquisition of a large number of high-resolution segmented tile images, at a magnification of ×100 for each tile (Figure 2B). Each optical field is focused automatically before image acquisition. The captured segmented tile images are automatically combined to construct a large image, with a total area of 20 × 20 mm. Since each tile segment can be magnified without the loss of high resolution, OBP-401–infected human tumor cells could be easily visualized with GFP signals in blood smears (Figure

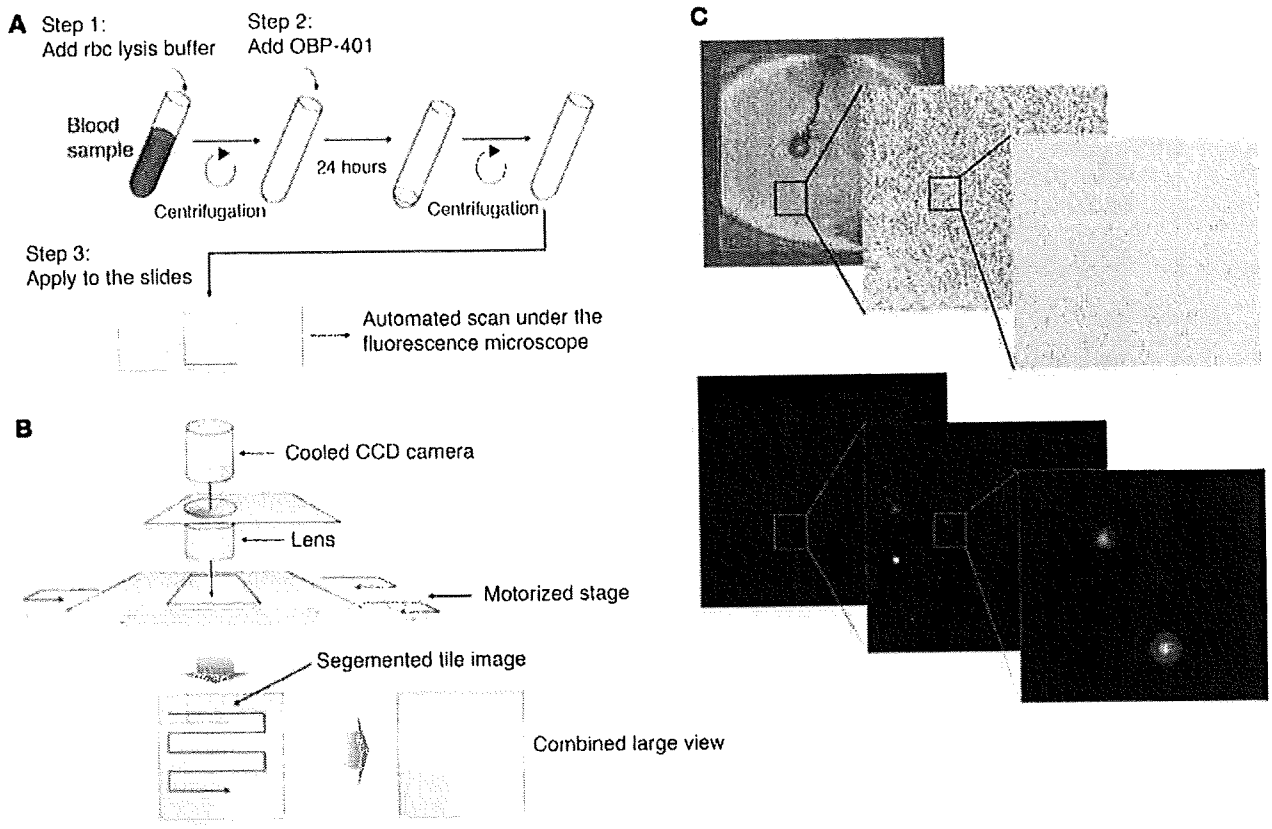

Figure 2
A simple method to detect telomerase-positive cells in the blood. (**A**) Steps in the sample preparation for GFP fluorescence detection. Blood samples (5-ml samples) are collected in heparinized tubes and incubated with rbc lysis buffer containing ammonium chloride (NH_4Cl) for 15 minutes. After centrifugation, cell pellets are mixed with 10^4 PFUs of OBP-401 and incubated at room temperature for another 24 hours. Cells are resuspended in 15 μl of PBS following centrifugation and then placed onto the slide under a coverslip. (**B**) System for automated fluorescence molecular imaging. The automated optical scan system serially captures segmented tile images in the area of the coverslip under fluorescence microscopy. (**C**) A high-resolution large view of the reconstructed tile images. The zoomed image allows easy visualization of GFP-expressing cells among millions of blood leukocytes. Original magnification, ×40 (left panels); ×100 (middle panels); ×400 (right panels).

2C). This automated microscopic scan system allows us to obtain high-magnification images with a large field of view.

Accuracy of CTC detection by ex vivo OBP-401 infection. To test the efficacy and accuracy of the system, whole blood samples from healthy donors were spiked with variable numbers of H1299 human lung cancer cells and then analyzed. Representative images of each sample are shown in Figure 3A. H1299 cells could be distinguished from the other blood cells even at lower magnification. The recovery of tumor cells was consistent over a target frequency range, between 10 and 1,000 cells spiked into 5 ml of blood from normal donors. Regression analysis of the number of GFP-positive cells versus the number of expected tumor cells yielded a correlation coefficient of $r^2 = 0.9996$ (Figure 3B). Thus, the number of GFP-positive cells reflects the actual peripheral blood tumor cell load. We also performed immunohistochemical analysis with anti-human CK-7/8 antibody to ensure that the cells labeled with GFP signals were indeed tumor cells. We used CK-7/8 as a marker for tumor cell detection, as H1299 cells were completely negative for CK-19 (Supplemental Figure 3). The automated microscopic scan system permits repeated scanning of the same fields repeatedly by a 2-dimensional line scanning technology. Merged images of fluorescent detection and CK-7/8 immunostaining confirmed that H1299 human lung cancer cells stably transfected with the *gfp* gene were CK-7/8 positive in the blood smear (Supplemental Figure 3). By using this dual imaging method, we confirmed that the GFP-positive cells were CK-7/8 positive following 24-hour exposure to OBP-401 and were distinguishable from other blood cells (Figure 3C). GFP-expressing cells were also morphologically classified as tumor cells (data not shown).

Comparative analysis of CTC detection by OBP-401, real-time RT-PCR, and flow cytometry. To compare the GFP-based CTC detection and other existing methods, blood samples spiked with variable numbers of H1299 cells were also analyzed. We performed real-time RT-PCR analysis with primers targeting the *hTERT* gene, as OBP-401–mediated GFP expression reflects the telomerase activity (Figure 1B). The number of GFP-positive cells was proportional to the increasing number of H1299 cells, between 10 and 1,000 cells in 5 ml of blood after ex vivo OBP-401 infection (Figure 3B); a significant increase in amplification, however, could not be observed even with 2,000 tumor cells in 1 ml of blood by real-time RT-PCR (Figure 4A), suggesting that the detected *hTERT* mRNA levels might be the background expression. In addition, a